Combustion and Flame 158 (2011) 69–90

Contents lists available at ScienceDirect

Combustion and Flame

journal homepage: www.elsevier.com/locate/combustflame

A combustion model for IC engine combustion simulations with multi-component fuels

Youngchul Ra *, Rolf D. Reitz

Engine Research Center, University of Wisconsin-Madison, United States

ARTICLE INFO

Article history:
Received 3 September 2009
Received in revised form 16 November 2009
Accepted 22 July 2010
Available online 12 August 2010

Keywords:
Multi-component fuel
Reduced mechanism
Auto-ignition
HCCI
Spray combustion
Internal combustion engines

ABSTRACT

Reduced chemical kinetic mechanisms for the oxidation of representative surrogate components of a typical multi-component automotive fuel have been developed and applied to model internal combustion engines. Starting from an existing reduced mechanism for primary reference fuel (PRF) oxidation, further improvement was made by including additional reactions and by optimizing reaction rate constants of selected reactions. Using a similar approach to that used to develop the reduced PRF mechanism, reduced mechanisms for the oxidation of *n*-tetradecane, toluene, cyclohexane, dimethyl ether (DME), ethanol, and methyl butanoate (MB) were built and combined with the PRF mechanism to form a multi-surrogate fuel chemistry (MultiChem) mechanism. The final version of the MultiChem mechanism consists of 113 species and 487 reactions. Validation of the present MultiChem mechanism was performed with ignition delay time measurements from shock tube tests and predictions by comprehensive mechanisms available in the literature.

A combustion model was developed to simulate engine combustion with multi-component fuels using the present MultiChem mechanism, and the model was applied to simulate HCCI and DI engine combustion. The results show that the present multi-component combustion model gives reliable performance for combustion predictions, as well as computational efficiency improvements through the use of reduced mechanism for multi-dimensional CFD simulations.

1. Introduction

As more attention is paid to methods for the reduction of pollutant emissions, detailed information about the combustion chemistry in engines is becoming critical for improving engine performance. In particular, in HCCI/PCCI engine research, where combustion is a chemical-reaction-governed process, the importance of accurate chemical kinetic mechanisms and their computational efficiency is emphasized.

Practical engine fuels consist of multi-components with different classes of chemical structures. For instance, gasoline and diesel consist of many different classes of hydrocarbons, such as paraffins, olefins, aromatics, and cycloalkanes, with a wide range of molecular weights. In addition, the exact composition of these fuels varies based on the source, distributor, and intended region and season of use. Because of the limitations of computational cost to deal with a large number of components in modeling the mixture preparation and subsequent combustion processes, most previous studies model the ignition/combustion characteristics of automotive fuels by representing them as blends of just two pure hydrocarbons (primary reference fuel), i.e., iso-octane and *n*-heptane, as a first approximation. However, as more detailed information about the combustion chemistry of the major components of the fuels and their effects on engine emissions is required for improving engine design, more attention is being paid to the inclusion of more realistic multi-component compositions in simulations.

Ideally, each fuel component requires its own set of combustion species and reactions. However, the resulting reaction mechanisms would be computationally prohibitive, even with current state-of-the-art computational facilities. Thus, it is usual to represent complex fuels in a class with a single, relatively simple, surrogate species that exhibits common combustion characteristics of the fuel class. For example, *n*-heptane is widely used as a surrogate for *n*-alkanes and iso-octane represents iso-alkanes.

Comprehensive detailed kinetic mechanisms have been compiled for certain fuels. For example, Curran et al. [1,2] developed mechanisms to study the oxidation of *n*-heptane and iso-octane. Fisher et al. [3] developed a detailed kinetic reaction mechanism that contained 264 species and 1219 reactions for methyl butanoate, which is regarded as a simple but representative surrogate for methyl esters (biofuels). A detailed mechanism for toluene (the smallest alkyl benzene) was developed by Bounaceur et al. [4],

* Corresponding author. Address: Engine Research Center, 1500 Engineering Drive, ERB #1016A, Madison, WI 53706, United States. Fax: +1 608 262 6707.
E-mail address: yra@wisc.edu (Y. Ra).

0010-2180/$ - see front matter © 2010 The Combustion Institute. Published by Elsevier Inc. All rights reserved.
doi:10.1016/j.combustflame.2010.07.019

and includes 148 species and 1013 reactions. Silke et al. [5] proposed a comprehensive reaction mechanism with 1081 species and 4269 reactions for oxidation of cyclohexane, which is the simplest representative cycloalkane. For the oxidation processes of C_{10}–C_{16} alkanes, Westbrook et al. [6] recently developed a complex reaction mechanism that consists of 2116 species and 8130 reactions.

These comprehensive mechanisms are very useful to give detailed information about reaction pathways. However, with reaction mechanisms that consist of several hundred species and several thousand reactions, it is still much too costly to use a detailed chemical kinetic mechanism directly in engine combustion studies using multi-dimensional CFD codes. It is necessary to develop chemical reaction mechanisms that retain the essential features of the fuel chemistry predicted by comprehensive reaction mechanisms, but with much improved computational efficiency in terms of memory usage and CPU time. The extent of comprehensiveness required depends on the computational resources available and the type of information desired from the simulation.

Significant effort has been made to develop reduced mechanisms for the oxidation chemistry of surrogates of conventional engine fuels. For example, Seshadri et al. [7] developed a skeletal mechanism with 23 species and 34 reactions for *n*-heptane oxidation and applied it to study the structure of premixed *n*-heptane flames. Peters et al. [8] developed a skeletal mechanism with 35 species and 56 reactions for *n*-heptane oxidation and further used it to derive global mechanisms for different temperature regimes by applying steady-state assumptions to many of the intermediate species. Hasse et al. [9] employed a reduced mechanism (29 species and 48 reactions) that includes reaction pathways involving intermediate hydrocarbon/oxygenate species for iso-octane oxidation in their study of the quenching of flames near cold walls.

Brakora et al. [10] developed a skeletal chemical reaction mechanism (41 species and 150 reactions) from the detailed methyl butanoate oxidation mechanism and combined it with a reduced *n*-heptane mechanism to give a reduced mechanism for biodiesel. Recently, Ra and Reitz [11] developed a reduced mechanism for PRF oxidation that consists of 41 species and 130 reactions. The mechanism was validated with measurements from shock tube tests, and HCCI and direct injection engine experiments available in the literature, which demonstrated the mechanism's reliable performance for combustion predictions, as well as computational efficiency improvements for multi-dimensional CFD simulations.

A number of researchers have modeled the chemistry of multi-surrogate fuel mixtures. Dagaut and Cathonnet [12] reviewed recent research on chemical kinetic modeling of kerosene combustion, as well as the relevant experimental studies. They surveyed a large body of experiments and kinetic modeling of kerosene combustion, showing how surrogate fuel mixtures, including an *n*-decane kinetic mechanism with aromatic and other species, can predict sooting behavior and overall heat release.

Buda et al. [13] discussed the importance of unified kinetic mechanisms for alkanes over both the low and high temperature regimes. Similarly, Ranzi et al. [14] proposed a "lumped approach" to generate mechanisms for *n*-decane, *n*-dodecane and *n*-hexadecane, and to reduce the size of each mechanism. They demonstrated that heavy *n*-alkanes displayed the same kinetic behavior in both high- and low-temperature regions and an overall kinetic scheme could be successfully extended directly.

Recently, the development of surrogate mixtures that represent gasoline and diesel combustion behavior was reviewed by Pitz et al. [15] and Farrell et al. [16], respectively. Pitz et al. described the general composition of gasoline in terms of fuel classes, viz, dominant component(s) in *n*-alkanes, iso-alkanes, naphthenes, olefins, aromatics, and oxygenates, which would be desirable surrogate components for gasoline. They further discussed the relative importance and availability of mechanisms for the major components in each class in terms of relevance to practical systems, understanding of the mechanisms, and property information. Farrell et al. [16] suggested that lower molecular weight surrogates would provide the most suitable basis for creating surrogate diesel fuels in the near term. The recommended surrogate components include *n*-decane, iso-octane, methylcyclohexane, and toluene. They also indicated the importance of liquid fuel vaporization processes in modeling the in-cylinder fuel/air/EGR mixture distribution in diesel engine combustion, emphasizing the lack of understanding of the implications of supercriticality with multi-component fuels. In addition, they stated that it is necessary to develop methods to generate substantially smaller mechanisms than those obtained from currently available reduction techniques, without sacrificing chemical comprehensiveness.

More recently, Puduppakkam et al. [17] reported a surrogate-blending technique and proposed a surrogate-fuel blend to represent a real gasoline fuel. In their model, detailed chemical-kinetics mechanisms for each component of the surrogate fuel were assembled and validated with kinetics experiments available in the literature. They further tested the model with HCCI engine experiments.

In the present study, a reduced chemical kinetic mechanism for the oxidation of representative surrogate components of typical multi-component automotive fuels is developed. Starting from an existing reduced mechanism for primary reference fuel (PRF) oxidation, further improvement is made to the performance of heat release and emissions predictions by including additional reactions and by optimizing reaction rate constants of selected reactions. Using a similar approach to that used for development of the reduced PRF mechanism, reduced mechanisms for oxidation of *n*-tetradecane, toluene, dimethylether (DME), ethanol, and cyclohexane are built and combined with the PRF mechanism and an existing reduced mechanism for methyl butanoate to form a multi-surrogate fuel chemistry (MultiChem) mechanism, which will be described in the following section. Validation of the present MultiChem mechanism is performed with ignition delay time measurements from shock tube tests and predictions by comprehensive mechanisms available in the literature.

A combustion model is also proposed to simulate engine combustion with multi-component fuels using the present MultiChem mechanism. In order to model the evaporation of multi-component gasoline and diesel sprays in engines, a discrete multi-component (DMC) vaporization model developed by Ra and Reitz [18] and tested for evaporation processes of single and multi-component fuel droplets and sprays in a constant volume chamber and engine combustion [19,20], is employed. In the vaporization model, unsteady vaporization of multi-component fuel droplets and sprays was considered for both normal and flash-boiling evaporation conditions. In addition, a characteristic diffusion length was defined to determine the amount of vaporized fuel as a function of time in order to treat surface phase change under trans-critical conditions. The physical properties of multi-component fuels were modeled using various correlations available in literature [21], as a function of temperature, composition and, if necessary, pressure.

Application of the model to simulate HCCI and DI engine combustion is also presented.

2. Mechanism reduction methodology

2.1. Reduction method

The basic aim of mechanism reduction is to identify unimportant species and reaction pathways in order to reduce the complexity of chemistry mechanisms and the number of variables, but still to maintain the important features of full schemes.

Various methods have been suggested to determine the importance of species and reaction pathways in a mechanism. Sensitivity analysis [22–25], a reaction elimination method [26], the method of detailed reduction [27], and chemical lumping techniques [28] are among the reduction methods that have been quite widely explored. Each method has its own disadvantages, as well as advantages. Automation of reduction procedures has drawn much interest as well. Soyhan et al. [29] developed an automatic reduction technique and applied it to reduce a natural gas mechanism, Montgomery et al. [30] have used the Computer Aided Reduction Method (CARM) to automate the mechanism reduction process, and more recently, the direct relation graph method [31] has been suggested and used to help automation of reduction procedures.

Patel et al. [32], Brakora et al. [10] and Ra and Reitz [11] used a combination of chemical lumping, graphical reaction flow analysis [33] and elimination methods to generate reduced mechanisms for the oxidation of *n*-heptane, methyl butanoate, and primary reference fuel, respectively, from more comprehensive reaction mechanisms. In the present study, the method used by Ra and Reitz is employed.

In the method, the reduction was performed using a combination of chemical lumping, graphical reaction flow analysis and elimination methods. It can be summarized in five steps: (1) identification of the most essential species and reaction steps of the base mechanism using graphical reaction flow analysis, (2) elimination of unimportant species and reactions from the base mechanism to obtain a new reduced mechanism, (3) tests of the new reduced mechanism at appropriate operating conditions and comparison of the profiles of species concentrations of selected species with reference data for validation, (4) modification of the reduced mechanism by adding/removing species and relevant reaction steps to/from the reduced mechanism or in order to improve the prediction of species concentration histories, and (5) optimization of the reaction rate constants of selected reactions to give the best agreement of ignition delay times with experimental measurements. In the final stage of the procedure, the results of sensitivity analysis are used to minimize the adjustment of reaction rate constants from those of the base mechanisms. For more details of the reduction methodology, readers are referred to Ref. [11].

2.2. Optimization of reaction rate constants

Once the reaction pathways of a reduced mechanism are established based on the reduction methods described above, the reaction rate constants of selected reaction steps can be optimized such that predicted ignition delay curves match experimental data or those of reference detailed mechanisms. In the present study, the reactions to be optimized in the reduced mechanism for each surrogate fuel were selected from the ignition delay curve sensitivity analysis. While conventional sensitivity analysis [34] assesses the temporal sensitivity of temperature and species concentrations to individual reaction steps during a single ignition process, the present approach enables an estimate of the global contribution of individual reaction steps to the ignition process over a wide range of temperature variation, such as that found during the compression stroke of HCCI engines. For the purpose of the study, the ignition delay time in a constant volume ignition process is defined as the time when a 400 K increase in mixture temperature above the initial temperature is reached. Among the six parameter variations explored by Ra and Reitz [11], two variations of pre-exponential factor, i.e., $k_1 = 2$ and $k_2 = 0.5$ times the base line value, were investigated in the present study, since this is sufficient to demonstrate sensitivities.

2.2.1. Sensitivity coefficients

An ignition delay sensitivity coefficient was calculated by changing the pre-exponential factor of the baseline value by the factors of k_1 and k_2, as $A = k \times A_{base}$. The equation to obtain the ignition delay sensitivity is

$$S_{ig}(T) = 100 \times \frac{(\log_{10} t_{k_1} - \log_{10} t_{k_2})}{\log_{10} t_{base} \log_{10}(k_1/k_2)} \quad (1)$$

where $S_{ig}(T)$ is the ignition delay sensitivity coefficient in percentile at initial temperature T, t_{k_1} and t_{k_2} are the ignition delay times obtained using the factors of k_1 and k_2, respectively, and t_{base} is the ignition delay time of the baseline case corresponding to initial temperature T. If S_{ig} is positive the ignition delay time shortens as the reaction rate (pre-exponential factor) increases.

The sensitivity of the gradient of ignition delay time to the variation of reaction rate of a selected reaction was also monitored. Based on the argument of Westbrook [35], the ignition delay time of the system can be reasonably formulated as $t_{ig} \sim ATe^{E^*/T}$, where A is a constant and E^* is the system activation energy. Therefore, the gradient of the logarithmic ignition delay times with respect to the initial temperature is given as $\frac{d \log t_{ig}}{dT} \sim \frac{1}{T} - \frac{E^*}{T^2}$. This indicates that gradient of the logarithmic ignition delay times is inherently a function of system temperature and activation energy and the influence of the system activation energy becomes more apparent as the system temperature decreases. Thus, at a given system temperature, the change of the temperature gradient of the logarithmic ignition delay times with respect to the variation of reaction rate of an individual reaction reflects the effect of the individual reaction on the system activation energy change.

Using the same change of pre-exponential factor as in the ignition delay sensitivity, the gradient sensitivity coefficient, $S_{gr}(T)$, is calculated as

$$S_{gr}(T) = \frac{\frac{d \log_{10} t_{k_1}}{dT} - \frac{d \log_{10} t_{k_2}}{dT}}{\log_{10}(k_1/k_2)} \times 100 \quad (2)$$

The unit of the gradient sensitivity is (s/K). Note that the variation of the ignition delay curve shape at a given temperature is obtained as an absolute change of the gradient of the ignition delay curves on the t_{ig}–T plot in a piecewise interval containing the temperature point of interest. Graphically, if S_{gr} is positive the ignition delay curve tends to rotate in counter-clockwise direction on the t_{ig}–T plot. The higher the absolute value of the gradient sensitivity, the more the ignition delay curve rotates.

In the present study, only newly added reactions were considered in the sensitivity analysis, since the C_0–C_3 stem reactions in the base PRF mechanism have been successfully validated in numerical models for engine studies [32,36,37] and were held in common in building the MultiChem mechanism. An example of the sensitivity method is given here for the tetradecane mechanism.

2.2.2. Sensitivity analysis of n-tetradecane auto-ignition

Figure 1 shows changes of the ignition delay curves corresponding to variations of the pre-exponential factors ($A = kA_{base}$, $k = 2.0$ and 0.5) for reactions that have significant effects on the oxidation process among those listed in Table 1. Also, sensitivity coefficient plots are presented for each reaction case considered. From Fig. 1a, for example, it can be seen that reaction class II affects dominantly the ignition delay times in low-to-NTC temperature regimes only ($T < 1000$ K). This is expected since the activation barrier of the reaction used in the mechanism is substantially low (−35 cal/mol-K) and the OH radicals govern the ignition process. The ignition delay sensitivity coefficients are large positive values in these temperature regimes, as shown in Fig. 1b, which indicates that the ignition delay curve transitionally shifts down significantly by increasing the reaction rate of the reaction class II of

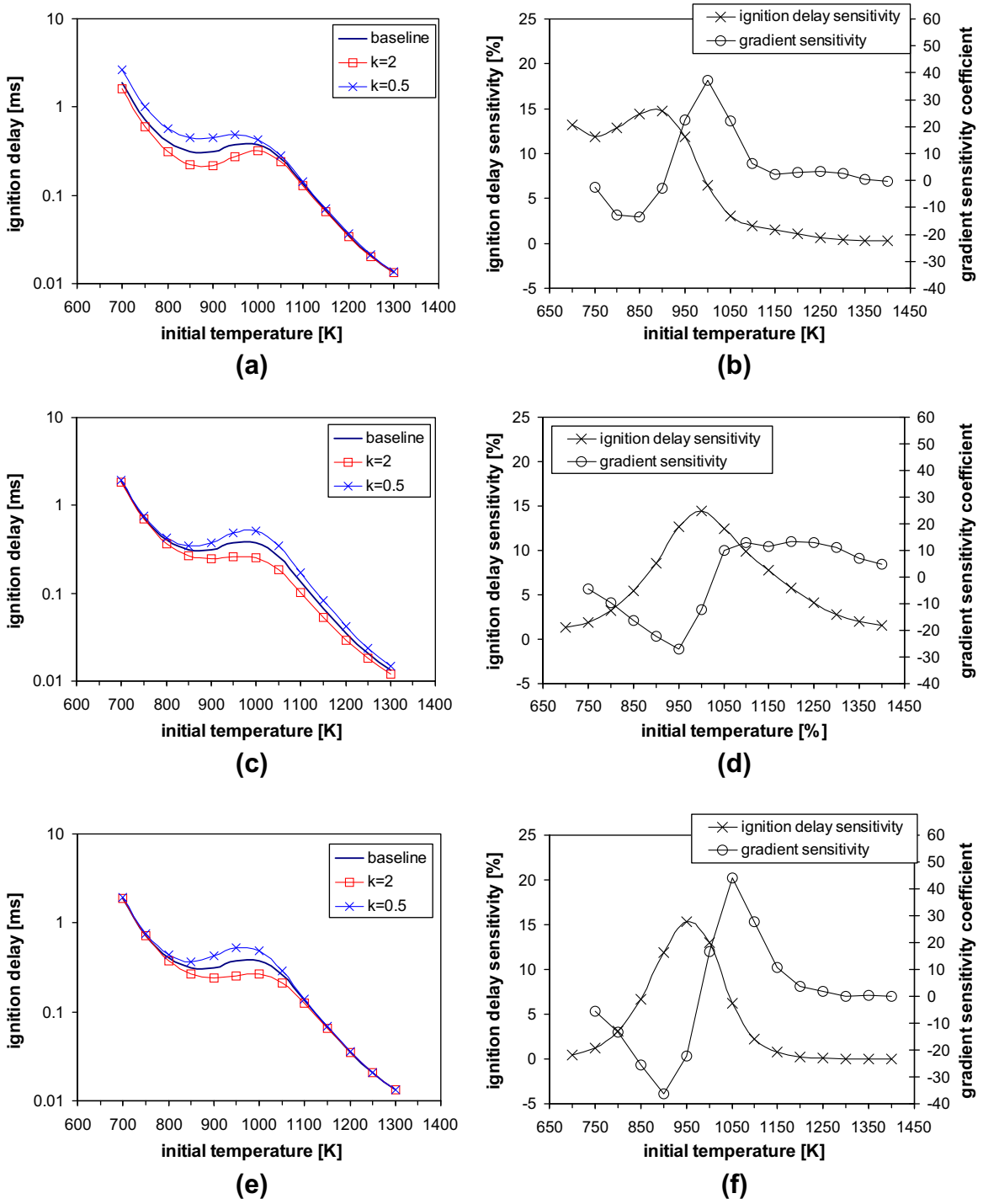

Fig. 1. Ignition sensitivity to variations of reaction rate constants of selected reactions of *n*-tetradecane oxidation. Stoichiometic *n*-tetradecane in air. $P = 40$ bar. (a and b) reaction class II, (c and d) reaction class III, (e and f) reaction class V, (g and h) reaction class VI, (i and j) reaction class VII, (k and l) reaction class IX, (m and n) reaction class X in Table 1.

the reduced *n*-tetradecane mechanism. The variation of the ignition delay curve in terms of the local slope of the curve is well presented by the corresponding variation of gradient sensitivity coefficients, changing from negative (clockwise rotation) to positive (counter-clockwise rotation) values.

As mentioned above, among the hydrogen atom abstraction reactions, abstraction by OH radicals (reaction class II) has a strong influence on ignition delay times in low-*T* and the NTC regimes of *n*-tetradecane oxidation. Reaction classes V and X, shown in Fig. 1e, f, k and l, mainly affect the temperature range of the NTC regime, while reaction classes III and IX influence both the NTC and high temperature regimes, significantly. It is notable that reaction classes V and X have the opposite effects in terms of the shifting direction of the ignition delay curves. Enhancing the β-scission reaction (class X) of *n*-tetradecyl radicals tends to inhibit the low-temperature branching that forms two OH radicals via ketoperoxide formation/decomposition reactions.

The characteristic effects of *n*-tetradecane oxidation reactions in most of the reaction classes shown in Table 1 are very similar to those reported for *n*-heptane [11], which indicates that a

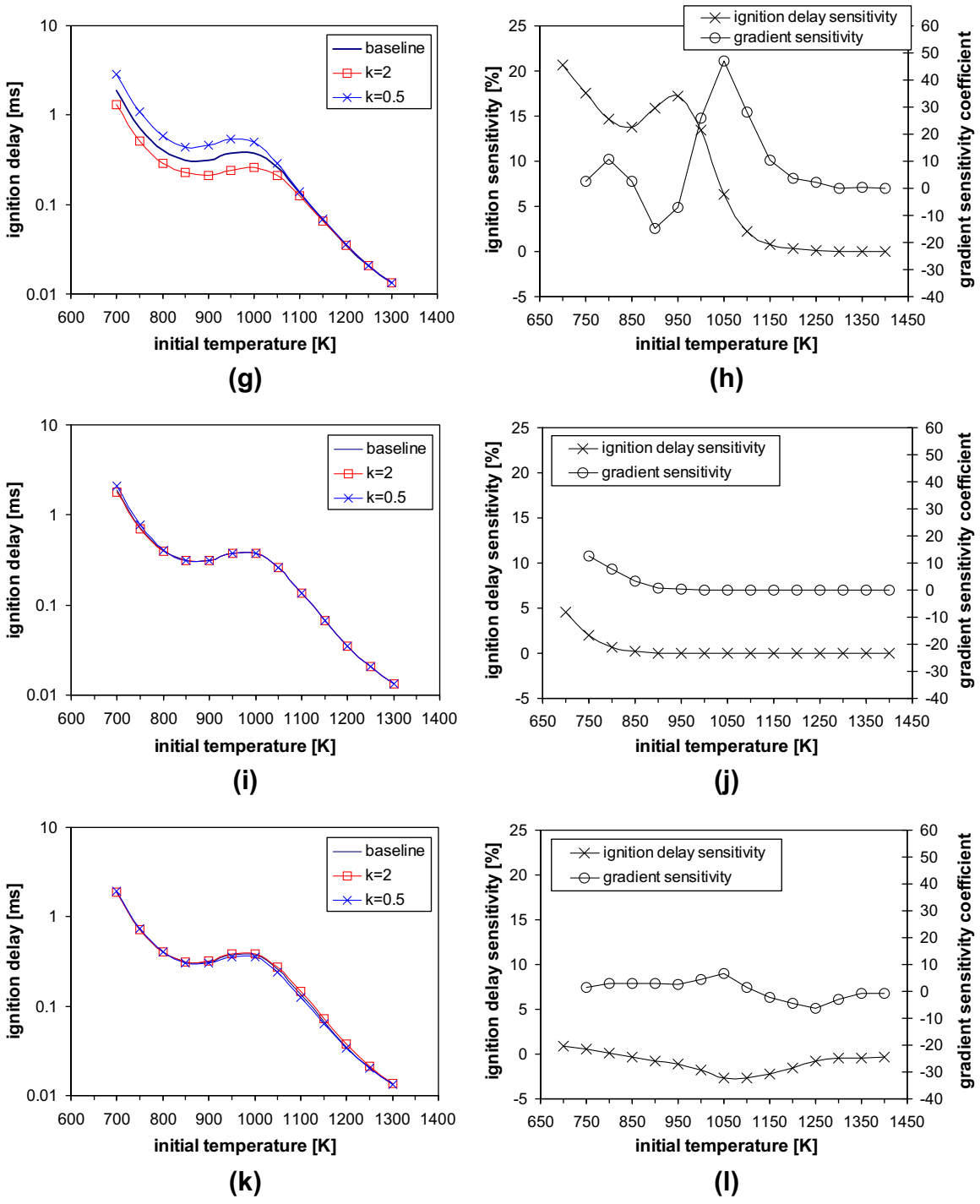

Fig. 1 (*continued*)

reduced mechanism can be adjusted for different fuels with similar chemical structures based on ignition delay curve sensitivity information. However, contrary behavior is seen for classes IV and V. Hydrogen atom abstraction by oxygen molecules (reaction class IV) has negligible influence in the present *n*-tetradecane oxidation, while it has a significant effect on the depth of the NTC regime in the *n*-heptane oxidation branch.

This is attributed to the greater complexity of the *n*-tetradecane reaction pathways in the present reaction mechanism. Note that *n*-tetradecane is assumed to also decompose to *n*-heptyl radicals in the present reaction mechanism. Thus, the reaction class X leads to another important level of alkyl ketoperoxide formation/decomposition reactions, which is C_7-ketoperoxide in the present reaction mechanism. This makes the effects of the reactions in the reaction classes shown in Table 1 become more complex than in the mechanism for lower C-number species oxidation.

It should be noted that the sensitivity coefficients results of the present ignition delay curves of the reduced mechanism may not be necessarily indicative of those of detailed mechanisms, because the reduced mechanism might not reflect some possible effects of omitted reaction pathways. Nevertheless, the sensitivity results of the reactions selected in the present study are believed to give

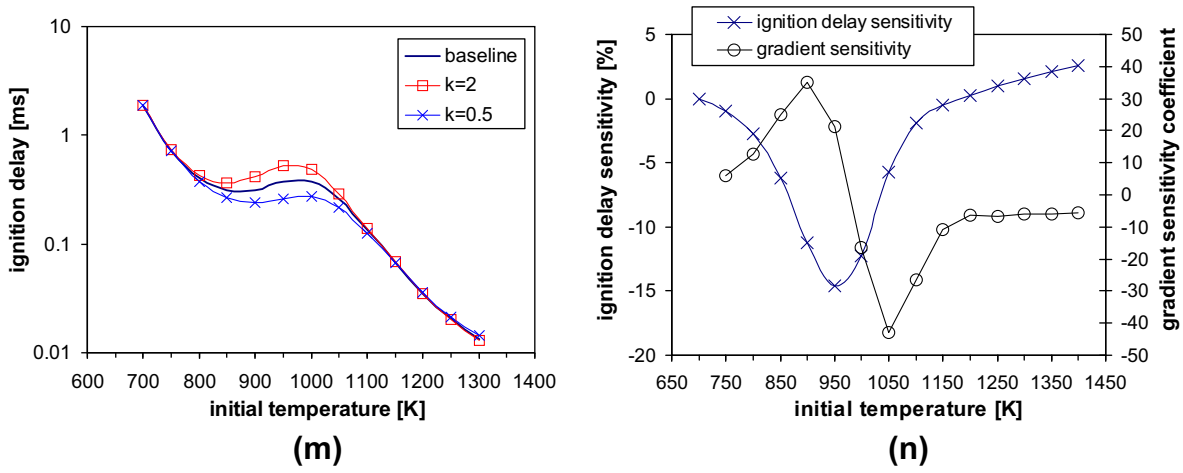

Fig. 1 (*continued*)

Table 1
Reaction classes modeled for low temperature oxidation of *n*-tetradecane. (S_1, S_2, S_3, X_1, X_2, X_3, Y_1,Y_2, Z_1, Z_2, and Z_3 are generic intermediate hydrocarbon species).

No.	Reaction	No. in Table A1	Class # in Ref. [1]
I	$RH + H = \dot{R} + H_2O$	21	2
II	$RH + OH = \dot{R} + H_2O$	22	2
III	$RH + HO_2 = \dot{R} + H_2O_2$	23	2
IV	$RH + O_2 = \dot{R} + HO_2$	24	2
V	$\dot{R} + O_2 = R\dot{O}O$	25	10
VI	$\dot{R}OO + O_2 =$ R-keto + OH	26	12, 22, 23
VII	R-keto = $CH_2O + R'CO$ + OH	27	24
VIII	$R'CO = R' + CO$	28	Low T branch + lower level ketoperoxides
IX	$\dot{R} = S_1 + S_2 + S_3$	29, 30	Low T branch + lower level ketoperoxides
X	$\dot{R} = Y_1 + Y_2$	31	Low T branch + lower level ketoperoxides
XI	$R' + (O/OH/CH_3) = R'' + (OH/H_2O/CH_4) + H$	35, 36, 37	Lower level H-abstraction
XII	$R' = X_1 + X_2 + X_3$	38	Low T branch + lower level ketoperoxides
XIII	$R'' = Z_1 + Z_2 + Z_3$	40, 41, 42	Lower level alkyl radical decomposition

important information about how the performance of a reduced mechanism can be optimized with minimal adjustment of reaction rate constants of the mechanism.

3. MultiChem mechanism formulation

Starting from an existing reduced mechanism for primary reference fuel (PRF) oxidation [11], further improvement was made by including additional reactions and by optimizing reaction rate constants of selected reactions. Using a similar approach to that used for development of the reduced PRF mechanism [11], reduced mechanisms for the oxidation of *n*-tetradecane, toluene, cyclohexane, dimethyl ether (DME), ethanol, and methyl butanoate (MB) were built and combined with the PRF mechanism to form the present multi-surrogate fuel chemistry (MultiChem) mechanism.

As base mechanisms to reduce for each surrogate component, detailed mechanisms were chosen, as shown in Table 2. In this section, the mechanism formulation of each surrogate component selected in this study is briefly mentioned. Detailed descriptions of mechanisms for each MultiChem surrogate component are provided in supplementary material [78].

It is notable that the present reduced mechanism does not share the full small molecule kinetics and themochemistry with the detailed mechanisms of interest, although the PRF base mechanism shares important major reactions and reaction pathways for small molecules with the detailed mechanisms and has been well validated against detailed mechanisms as well as experimental data with concentration profiles of selected species. This may lead to potential discrepancy of performance between the reduced and the detailed mechanisms. Also, the effects of the kinetics of small molecules missing in the reduced mechanism may depend on the

Table 2
Detailed mechanisms selected to be the base mechanisms for the reduced mechanism for surrogate fuel components considered in the present study.

Surrogate component	Fuel family represented	Base detailed mechanism	No of species and reactions (species, reaction)	
			Detailed mechanism	Present mechanism
n-Tetradecane	Heavy alkanes	Westbrook et al. [6]	(1668, 6449)	(47, 181)
Toluene	Aromatics	Bounaceur et al. [4] and Andrae et al. [42]	(148, 1036) (1083, 4635)	(50, 255)
Cyclohexane	Napthenes	Silke et al. [5]	(1081, 4269)	(67, 287)
Dimethyl ether	Ethers	Curran et al. [58,59]	(79, 351)	(27, 96)
Ethanol	Alcohols	Marinov [55]	(57, 383)	(27, 117)
Methyl butanoate	Esters	Fisher et al. [3]	(264, 1219)	(42, 178)

reaction conditions. Since the present reduced mechanism mainly focuses on low temperature regime, discrepancies of predicted results between the reduced and detailed mechanisms may become larger at high temperature conditions. The authors leave the possible further improvement of the present reduced mechanism in the high temperature regime for future study.

3.1. Primary reference fuel (PRF) mechanism

In order to make a more robust common pathway of low-C hydrocarbon oxidation, which is important in extending the range of fuel components included in the reduced mechanism to other surrogate fuels, certain reaction pathways involving C_3 intermediate species in the PRF mechanism were updated to improve the prediction of UHC emissions speciation in HCCI operation under various equivalence ratios, especially for rich mixtures. In the original PRF mechanism [11], less attention was paid to the speciation of UHC emissions of HCCI operation at rich conditions and the underprediction of C_2H_2 and over-prediction of CH_4 were found to influence significantly the soot modeling that employs C_2H_2 as an inception species. By improving the prediction of gas phase reactions related to formation of C_2H_2, the reduced mechanism could capture emissions characteristics much better without any cost of performance of ignition timing prediction.

Four more reactions that involve propene (C_3H_6) and active radicals were added and five more reactions were added to supplement propenyl (C_3H_5) reaction pathways. In addition, five more reactions of C_3H_4 (methylacetylene or propadiene) oxidation were added. Ethane oxidation pathways were improved, as well, by adding two reactions to consider the ethylperoxide formation pathways and two H-atom abstraction reactions by H and CH_3 radicals. Ethylene oxidation was supplemented with the addition of two H-atom abstraction reactions by H and O_2 molecules and one O-atom addition reaction to form CH_3 and HCO. In addition, a pressure-dependent decomposition reaction of methoxy (CH_3O) radicals to form formaldehyde and H-atom, and a reaction of CH_2CO with OH to form CH_3O + CO were added to improve the performance of the reduced mechanism. Finally, the reaction rate constants of several CH_4 oxidation reactions were updated with those in a more recent detailed mechanism [38].

3.2. n-Tetradecane mechanism

Due to its relative abundance in the composition and the closeness of the physical properties to those of typical diesel fuels [39], it is reasonable to select *n*-tetradecane as one of the major surrogate components to represent the chemical kinetics as well as the physical properties of diesel-like fuels. With the *n*-tetradecane reaction branch (1668 species, 6449 reactions) in the parent comprehensive mechanism by Westbrook et al. [6,40] being used as a base mechanism (see Table 2), the basic reactions pathways of the reduced *n*-tetradecane mechanism were formulated according to the generic form of the reaction equations that were developed for *n*-heptane and iso-octane oxidation. As part of the mechanism, twelve major reaction pathways were used to describe the low-temperature reaction branches from *n*-tetradecane to intermediate hydrocarbon species that contain up to three carbons. Basically, one chemical reaction equation was assigned to each step of the generic form of the reaction equations, as shown in Table 1, except for reaction class IX and XIII. Two and three reactions were assigned to reaction classes IX and XIII, respectively, to ensure various decomposition species from the radical. In order to make the reaction pathway between C_{12}-species and C_3-species, reduced sub-mechanisms for oxidation of *n*-pentene (C_5H_{10}) and butenyl

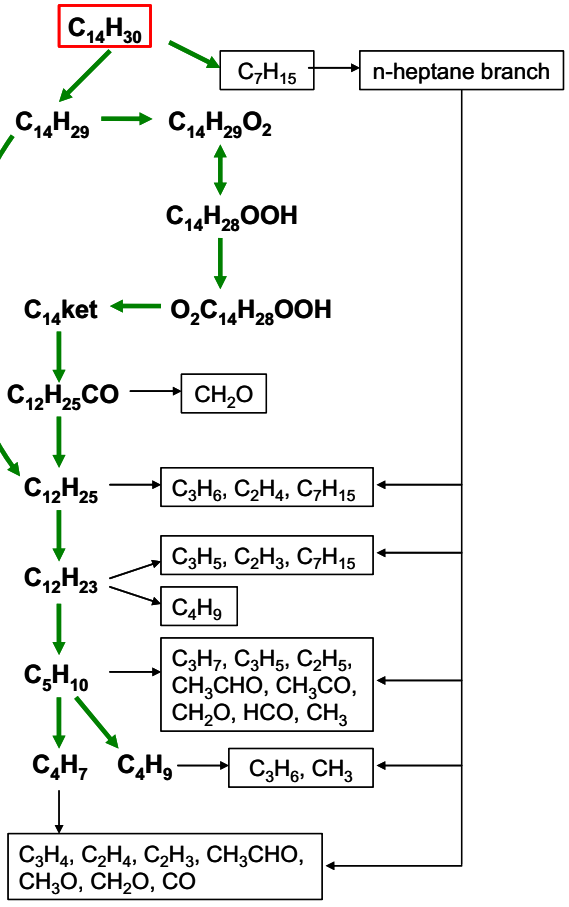

Fig. 2. Major reaction pathways of tetradecane oxidation.

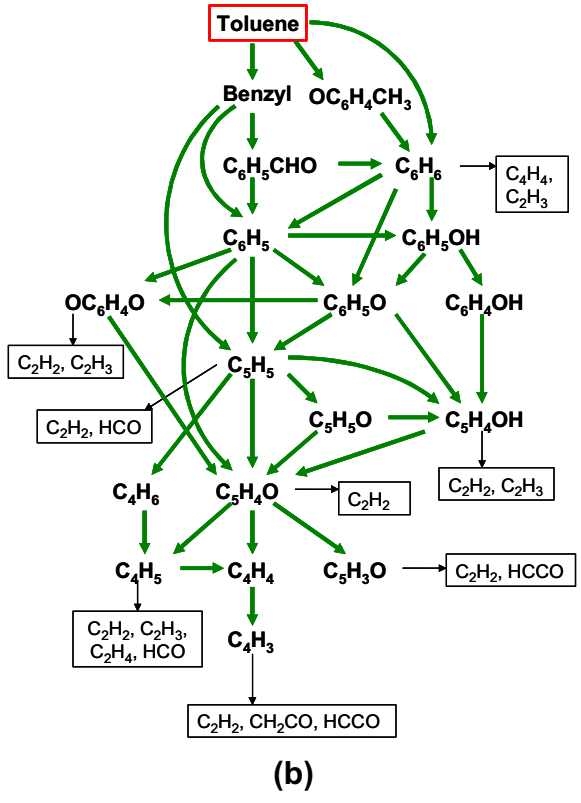

Fig. 3. Major reaction pathways of toluene oxidation.

(C_4H_7) were included in the present mechanism, as shown in Fig. 2. Overall, a total of 11 species and 35 reactions were added to the base PRF mechanism to generate the *n*-tetradecane oxidation branch in the present reaction mechanism. The detailed reactions and their rate constants are listed in Table A1 [78].

3.3. Toluene mechanism

Toluene is the most abundant aromatic hydrocarbon in gasolines (up to 10%), with a research octane number of 120 [39]. Although it was reported by Roubaud et al. [41] that the type of aromatic present in practical engine fuels influences auto-ignition at low temperatures, as a first approximation the simple chemical structure and oxidation reaction pathways of toluene are regarded to be well representative of the characteristics of aromatic fuels. Based on the mechanisms by Bounaceur et al. [4] and Andrae et al. [42], the major reaction pathways which include primary toluene oxidation pathways and subsequent secondary reactions were modeled in the present study. The primary reaction pathways are simplified as two reaction flows from toluene: (1) toluene to benzaldehyde, and (2) toluene to benzene. The secondary reaction pathways are involved with phenyl radicals and benzene to give lower C-number hydrocarbon species and radicals. In the present study, the reactions for C_3–C_6 hydrocarbons such as C_5H_5, C_4H_5, C_4H_4, C_4H_3, etc., were adopted from the benzene oxidation mechanism of Bounaceur et al. [4], and combined with the C_0–C_3 hydrocarbon reactions of the base PRF reaction mechanism [11]. A total of 20 species and 121 reactions were added to the base PRF mechanism to account for aromatics in the present MultiChem mechanism, as shown in Fig. 3, and the reactions and their rate constants are listed in Table A1 [78]. Note that the number of species and reactions added to the base mechanism is relatively large compared to those for other components considered in the present study. This is due to the fact that toluene has a ring structure while other components mainly have straight chain structures. Due to this characteristic structure, the toluene oxidation process involves ring-opening stages. This leads to substantially different reaction pathways and intermediate species from those of other components.

3.4. Cyclo-hexane mechanism

Cycloalkanes are an important chemical class of hydrocarbons that make up a significant portion in diesel (up to ~35%), jet (up to ~20%), and gasoline (up to ~10%) fuels [15,16]. As a representative surrogate for cycloalkanes, cyclohexane was chosen, since not

Table 3
Cyclohexane ring-opening reactions modeled in the present reaction mechanism.

Ring-opening reaction	Combined reactions	Reaction in the present mechanism
$cyOC_6H_9O = OC_5H_8CHO$	NA	$cyOC_6H_9O = OC_5H_8CHO$
$cyC_6H_9O = C_5H_8CHO$	$C_2H_2 + C_3H_6CHO = C_5H_8CHO$	$cyC_6H_9O = C_2H_2 + C_3H_6CHO$
$HOOC_5H_8CHO + OH = cyO_2C_6H_{10}OOH$	$cyC_6H_{11}O_2 = cyC_6H_{10}OOH$ $cyC_6H_{10}OOH + O_2 = cyO_2C_6H_{10}OOH$	$cyC_6H_{11}O_2 + O_2 = HOOC_5H_8CHO + OH$
$C_5H_{10}CHO = cyC_6H_{11}O$	$C_5H_{10}CHO = C_2H_4 + C_3H_6CHO$	$cyC_6H_{11}O = C_2H_4 + C_3H_6CHO$
$C_6H_{11} = cyC_6H_{11}$	NA	$C_6H_{11} = cyC_6H_{11}$
$C_6H_{10}OOH = cyC_6H_{10}OOH$	$cyC_6H_{11}O_2 = cyC_6H_{10}OOH$ $C_4H_6OOH + C_2H_4 = C_6H_{10}OOH$	$cyC_6H_{11}O_2 = C_4H_6OOH + C_2H_4$

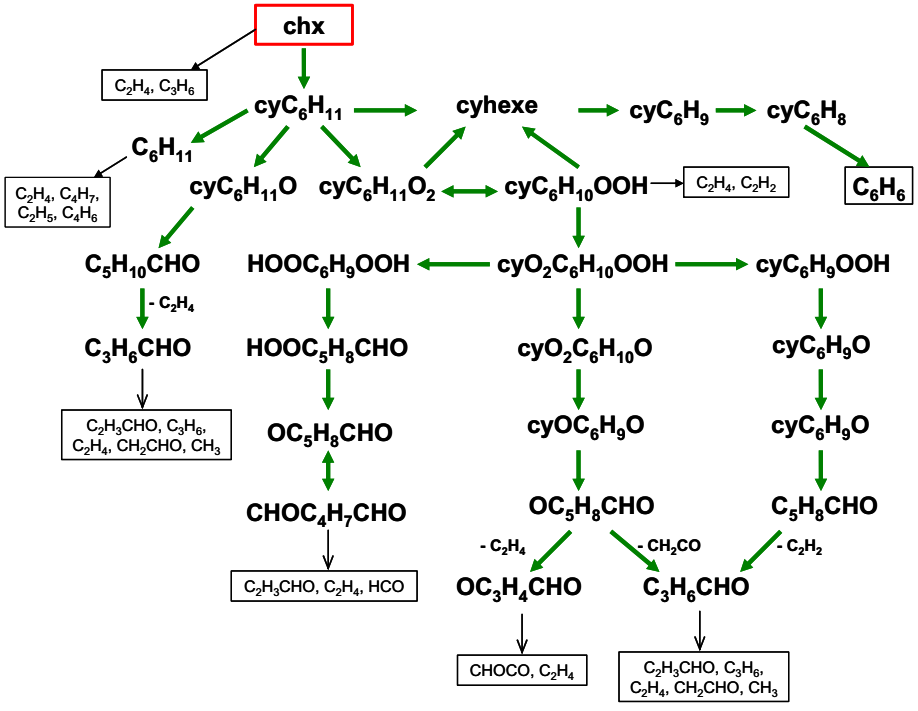

Fig. 4. Major reaction pathways of cyclohexane oxidation.

only there are many experimental data [43–48] and detailed kinetic mechanisms [5,45,49–51] available in the literature, but also it is believed that cyclohexane, as the simplest cycloalkane, can represent the major reaction characteristics of cycloalkane oxidation processes [5].

In the present study, the comprehensive mechanism (1081 species, 4269 reactions) by Silke et al. [5] was used as the parent mechanism. The general features of cyclohexane oxidation are that cyclohexane oxidizes at high temperatures mainly via unimolecular decomposition leading to linear products, H-atom abstraction leading to both dehydrogenation and formation of benzene, and β-scission reactions that break the cyclic ring. At lower temperatures, the dominant reaction path for cyclohexane is H-atom abstraction from the parent fuel molecule by OH, HO_2, and other radicals, followed by successive additions of oxygen leading to chain-branching pathways of the NTC region.

Among the ring-opening reactions modeled in the comprehensive mechanism, a total of six ring-opening steps were considered in the present reaction mechanism, as listed in Table 3. In the table, the reactions from the comprehensive mechanism that were combined are listed, as well. Some of the ring-opening reactions were combined with other reactions to make reduced steps in the present reaction mechanism. A total of 17 species and 53 reactions to describe cyclohexane oxidation were added to the base PRF mechanism to form the present MultiChem mechanism, as shown in Fig. 4 and listed in Table A1 [78].

3.5. Ethanol mechanism

Important intermediates of the oxidation process of alcohols have been identified as acetaldehyde, acetic acid, formaldehyde, and formic acid by many researchers [52,53]. Among them, acetic acid and formic acid are attributed to minor reaction pathways [54]. Much of the chemistry for alcohol compounds should be relevant to ethanol [54], where reaction pathways include most of the important characteristic oxidation processes of alcohols. Therefore, ethanol was selected as a surrogate fuel to represent the alcohols.

A detailed reaction mechanism of Marinov [55] with 57 species and 383 reactions was used as the base ethanol mechanism. From a flux analysis four major reaction pathways were identified. The major reaction pathways include dominant reactions at high and low temperatures. With further eliminating relatively unimportant reaction pathways from the reduced mechanism at no significant expense of computational accuracy, four species (ethanol, CH_3CHOH, CH_3CH_2O, CH_3CHO) and 31 reactions were newly combined with the base PRF mechanism to generate the MultiChem mechanism, as shown in Fig. 5 and listed in Table A1 [78].

3.6. Dimethyl ether (DME) mechanism

The C–O bond energy (~362 kJ/mol [56]) is smaller than that of the C–H bond (~407 kJ/mol [56]) and the distortion of the C–O bonds in the DME molecule weakens the bonding strength. Thus, the C–O bond breaks easier than the C–H bond. This enables the chain reaction to start at relatively low temperatures, which leads to the low auto-ignition temperature. In addition, its simple chemical structure that has no C–C bond to act as a seed for polymerization, which leads to polyaromatic hydrocarbons, and its high oxygen content enable substantial reduction of particulate matter at a slight expense of NOx [57].

In the present study, a comprehensive reaction mechanism of Curran et al. [58,59] was used as the base DME mechanism. In order to model DME's primary reaction pathways, a total of eight additional species and 36 additional reactions were newly coupled with the stem reactions for the low-C-number hydrocarbons employed in the MultiChem mechanism, as shown in Fig. 6 and listed in Table A1 [78].

3.7. Methyl butanoate (MB) mechanism

It is believed that the overall oxidation characteristics of biodiesel can be reasonably represented by those of simpler surrogate fuels that are in the same ester class [60,61]. One of the simplest fuels that has been used as a biodiesel surrogate for kinetic modeling is methyl butanoate (MB, $CH_3CH_2CH_2(C{=}O)OCH_3$), which contains the essential chemical structure of the long-chain fatty acids and a shorter, but similar, alkyl chain.

Brakora et al. [10] developed a skeletal chemical reaction mechanism (41 species and 150 reactions) and validated it for multi-dimensional engine combustion simulations. The reduced mechanism was generated from the detailed methyl butanoate oxidation mechanism (264 species and 1219 reactions) of Fisher et al. [3]. Adopting the reduced MB mechanism by Brakora et al. with minor modification of pathways in the present study, a total of nine species and 44 reactions were newly added to the present MultiChem mechanism to describe the MB oxidation pathways, as listed in Table A1 [78].

3.8. Co-oxidation reactions

There is no general information available about the importance of co-oxidation reactions of fuel components in the combustion chemistry of a blended or multi-component fuel. Several researchers [62–65] found that co-oxidation reactions between the individual fuel components were important and the range of co-oxidation reactions depended on the variety of species used in the mechanism. However, it has also been suggested that interactions between the fuel components are unimportant and it is possible to develop a reduced mechanism for mixtures by combining the reduced mechanisms of the single components [64].

In the present study, several co-oxidation reactions between the surrogate components were considered in order to take the possible contribution of those reactions into account without any significant additional computational cost (no additional number of species). Since only dominant reaction pathways described with single lumped species were used to model the branching reactions for each surrogate fuel considered in the present study, only co-oxidation reactions that involve the radicals produced from one of the fuels through H-atom abstraction (e.g., alkyl, benzyl, and cyclohexyl radicals) and the other fuels, $R_1 + R_2H \leftrightarrow R_1H + R_2$, were included in the reduced mechanism. According to the argument by Andrae et al. [62], co-oxidation reactions between similar fuels

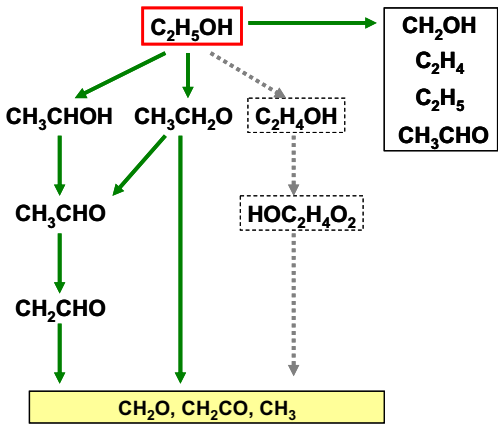

Fig. 5. Major reaction pathways of ethanol oxidation.

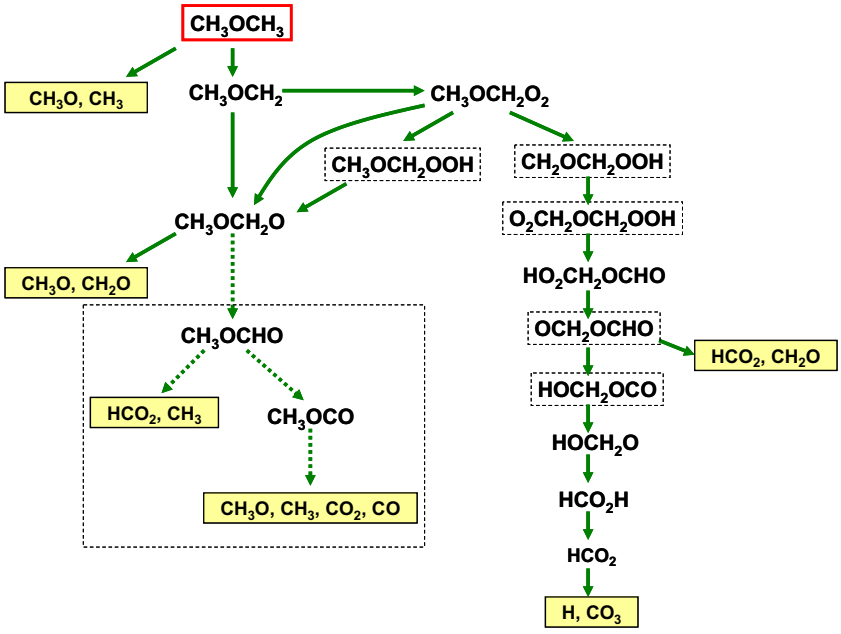

Fig. 6. Major reaction pathways of dimethy ether (DME) oxidation.

only need be considered, and co-oxidation reactions between fuels that are substantially different can be neglected. Other co-oxidation reactions such as those between fuels and alkylperoxy radicals are not included in the present work, but may be added later to enhance the completeness of the co-oxidation pathways. The rate constants for the co-oxidation reactions were set to those used for the PRF mechanism by Ra and Reitz [11] and listed in Table A1 [78].

With reactions pathways for the surrogate components considered in the present study combined together, the final version of the MultiChem mechanism consists of 113 species and 487 reactions, as shown in Table A1 [78].

3.9. Thermodynamic properties

The thermodynamic properties of species considered in the present reaction mechanism are based on those used in the parent mechanisms. When a generic species was selected to represent its isomers the thermodynamic data of the species that existed most in the oxidation process were used for its properties. In this way, the consistency of the thermodynamic properties between the reduced and parent mechanisms was maintained as much as possible. Similarly, transport properties of species can be set, although no transport properties were used in the present study since validation was performed for auto-ignition only.

4. Experiments for comparison

4.1. Ignition delay time experiments

Ignition delay predictions using the present reaction mechanism were validated using experimental data available in the literature. For the *n*-tetradecane mechanism, experimental measurements of ignition delays at pressures close to engine combustion conditions are very rare. Shen et al. [66] recently reported ignition delay measurements of *n*-tetradecane/air mixtures in

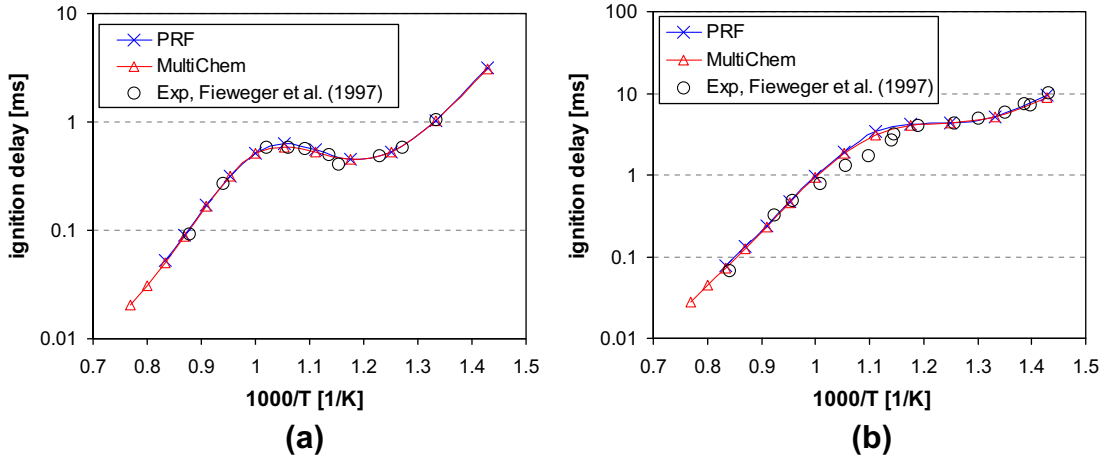

Fig. 7. Comparison of ignition delay time predictions between the present MultiChem mechanism and the reduced PRF mechanism [11] for various initial temperatures. The initial pressure was 40 bar. Shock tube tests are from Ref. [75]. (a) Stoichiometric iso-octane/air mixtures, (b) stoichiometric *n*-heptane/air mixtures.

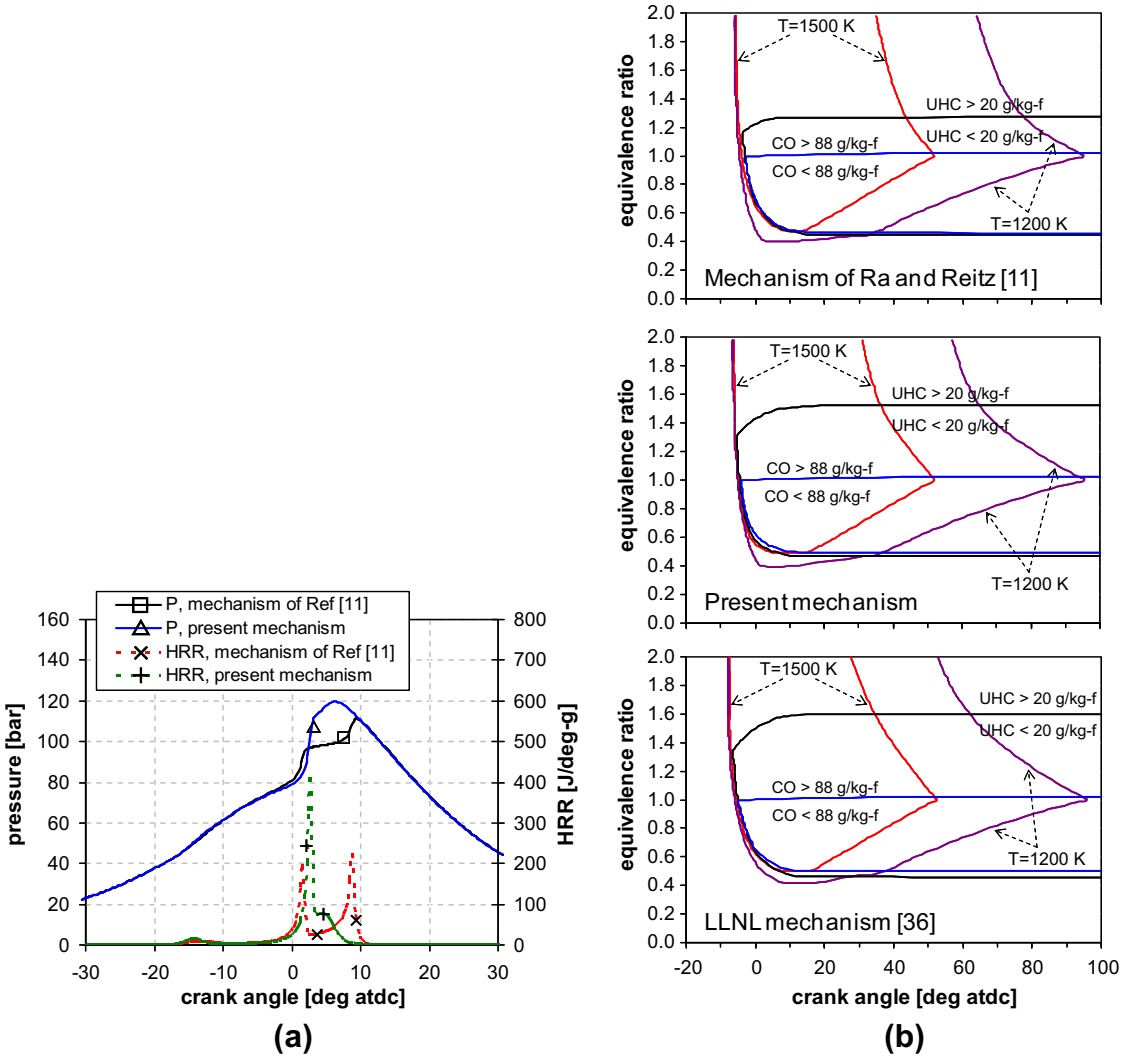

Fig. 8. Improvement of PRF mechanism in the MultiChem mechanism. (a) Pressure and HRR profiles of HCCI combustion of PRF0 under a medium load low temperature combustion condition (O_2 = 8.58%, $\phi_{overall} \sim 0.68$, engine speed = 2000 rev/min), (b) Comparison of emissions and gas temperature predictions of HCCI combustion (EGR = 50%) among the LLNL detailed mechanism [38], the PRF mechanism by Ra and Reitz [11], and the PRF mechanism in the present study.

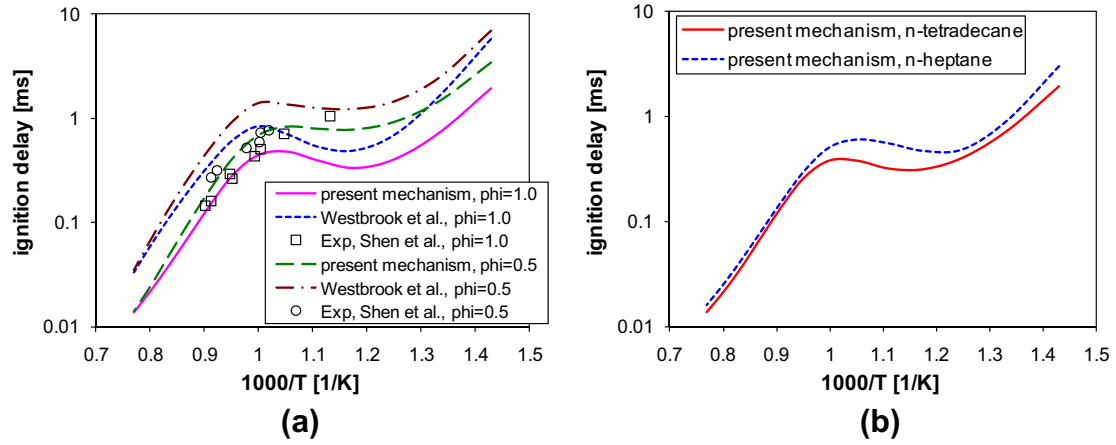

Fig. 9. Comparison of prediction of ignition delay times of *n*-tetradecane oxidation at constant volume between the present reaction mechanism and shock tube test data [66] and prediction by detailed mechanisms [6]. (a) Ignition delay times of *n*-tetradecane/air mixtures at 40 bar initial pressure, (b) comparison of ignition delay times between stoichiometric *n*-heptane/air and *n*-tetradecane/air mixtures at 40 bar initial pressure.

shock tube tests at intermediate-to-high temperatures and elevated pressures for two different equivalence ratios. This experimental data was used for validation of the *n*-tetradecane oxidation predicted by the present reaction mechanism.

For the toluene mechanism, three shock tube experimental researches were employed; experiments by Bounaceur et al. [4] for high temperature toluene/O_2/Ar mixtures, by Davidson et al. [67] for toluene/air mixture at intermediate-to-high temperatures, and by Herzler et al. [68] for *n*-heptane/toluene/air mixtures at low-to-intermediate temperatures.

In order to validate the performance of the reduced cyclo-hexane mechanism, rapid compression machine (RCM) data by Lemaire et al. [45] and shock tube test data by Daley et al. [43] were used. The RCM data, which was originally obtained in pressure range of 11–14 atm, was scaled to 12.5 bar using the pressure scaling proposed by Daley et al., ignition delay, τ–$P^{-1.1}$, in order to be combined with the shock tube data by Daley et al.

For validation of the DME oxidation reactions of the present reaction mechanism, shock tube tests by Pfahl et al. [69] were used. In the experiments, ignition delay times of stoichiometric DME/air mixtures were measured at two different initial pressures, one of which is close to engine conditions.

For the MB mechanism, shock tube tests by Dooley et al. [61] were used for validation. In the experiments, high temperature MB/O_2/Ar mixtures with various equivalence ratios were tested at two different reflected shock pressures. In the present study the measurements at 4 atm reflected shock pressure were used. For validation of the ethanol mechanism as an individual component, predictions using the corresponding detailed mechanisms were compared with those by the present reaction mechanism.

Auto-ignition measurements in shock tube tests by Gauthier et al. [70] were used to validate the performance of the present reaction mechanism for ignition predictions of gasoline surrogate mixtures.

They tested two ternary surrogate mixtures consisting of iso-octane, toluene, and *n*-heptane; Surrogate-A (63/20/17%) and surrogate B (69/14/17%) by liquid volume, as well as RD387 gasoline (see Table D1 [78]). The measured ignition delay times of gasoline/air and ternary surrogate/air mixtures for various temperatures, equivalence ratios and pressures were compared with the predicted values using the same ternary surrogate fuels proposed by Gauthier et al.

Also, based on the measured composition of RD387 gasoline [70], a 4-component surrogate model is proposed in the present study and its ignition delay predictions were compared with the measured data. Ten major components of the gasoline, i.e., cyclopentane, toluene, ethylbenzene, *m*-xylene, *n*-pentane, *n*-heptane, isopentane, 3-methylhexane, 2-methylhexane and iso-octane are grouped into four surrogate components (cyclohexane, toluene, *n*-heptane and iso-octane) according to their chemical classes.

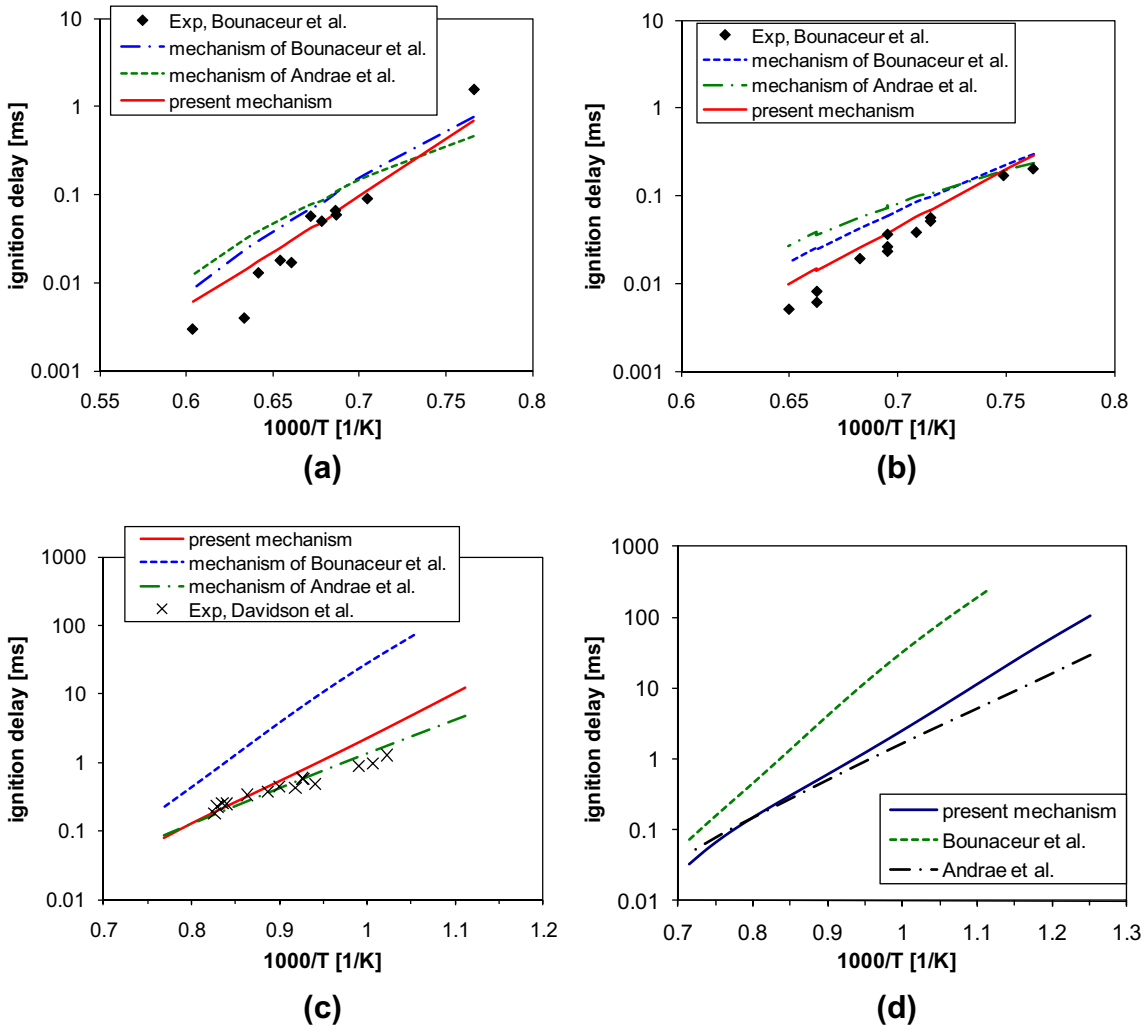

Fig. 10. Comparison of prediction of ignition delay times of toluene oxidation at constant volume between the present reaction mechanism and experimental data [4,67] and prediction by detailed mechanisms [4,42]. (a) Ignition delays of toluene/O_2/Ar mixtures at equivalence ratio of 1.0 and pressures of 7–9.5 bar, (b) ignition delays of toluene/O_2/Ar mixtures at equivalence ratio of 0.5 and pressures of 7–9.5 bar, (c) ignition delays of stoichiometric toluene/air mixtures at 50 bar, (d) ignition delays of stoichiometric toluene/air mixtures at 40 bar.

For detailed information about the composition of the gasoline and model surrogate fuel, refer to Ref. [70] and Table D1 [78]. Since the grouping method employed in this study does not adjust the proportion of individual surrogate components, the average properties of the surrogate mixtures may be different from the target mixtures. For example, the average molecule weight and H/C ratio of the 4-component surrogate mixtures are 96.6 and 1.95, respectively, while those of the RD387 (assuming the major components represent the entire composition) are 86.5 and 1.84, respectively. However, this approximation was considered to be reasonable.

4.2. HCCI engine experiments

In order to test the present mechanism in homogeneous charge compression ignition engine simulations, experiments by Puduppakkam et al. [17] were employed. Among the fuels with which they performed engine tests, the 4-component gasoline surrogate fuel was considered for validation of the reduced mechanisms of the present study. Also, 5-component model-fuel blend was derived from their 7-component model-fuel blend since some of the fuel components considered in Ref. [17] were not modeled in the present reaction mechanism and tested for HCCI combustion. In this case, isohexane was merged into iso-octane and styrene into toluene. Methycyclohexane was modeled using cyclohexane. 1-Pentene was modeled using a submechanism of *n*-tetradecane oxidation in the present study. The details of model composition of the fuels is listed in Table D2 [78], along with the composition proposed by Puduppakkam et al. [17]. Details of the engine are given in Table D3 [78].

4.3. DI diesel engine experiment

Finally, in order to demonstrate the performance of the reduced mechanism for spray combustion applications, low temperature combustion (LTC) compression-ignition experimental results from a direct-injection, light-duty diesel engine were used [71]. In the experiments, the distillation and fuel composition in classes were measured, as well as profiles of cylinder gas pressure for combusting cases. Detailed specifications of the engine are given in Ref. [72]. The fuel specifications and operating conditions of the engine experiment simulated in this study are given in Table D4 [78].

5. Results and discussion

The performance of the present MultiChem mechanism was tested by comparing the predicted results with experimental data

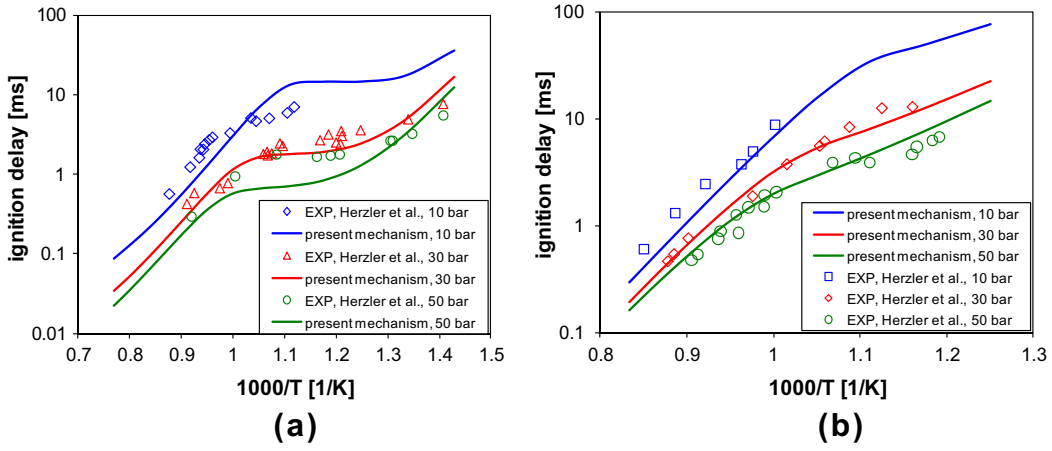

Fig. 11. Comparison of prediction of ignition delay times of *n*-heptane/toluene/air mixtures with experimental data. Experiments by Herzler et al. [68]. Mixtures of 35% *n*-heptane and 65% toluene by volume. Ignition delays (a) at $\phi = 1.0$ and (b) at $\phi = 0.3$.

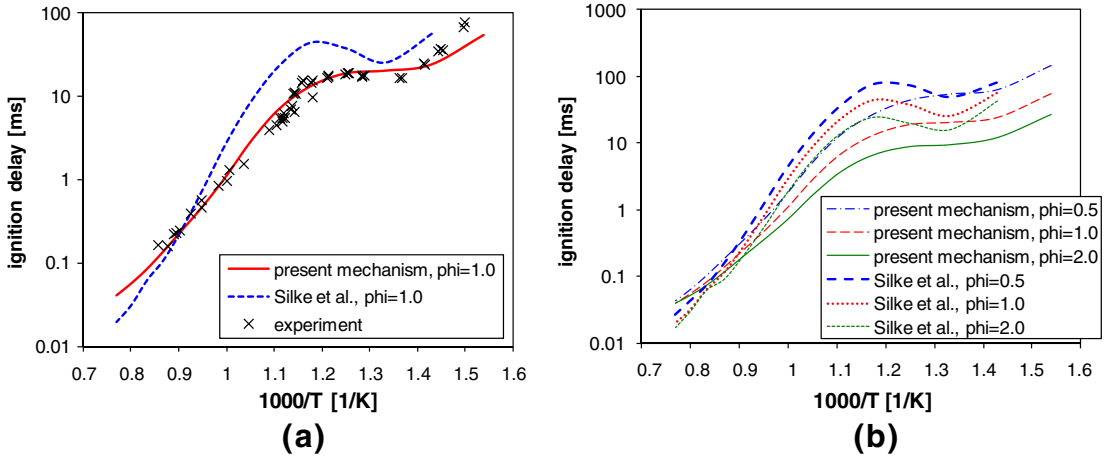

Fig. 12. Comparison of prediction of ignition delay times of cyclohexane/air mixtures at constant volume with experimental data and a detailed mechanism. Initial pressure is 12.5 bar. (a) Comparison with experiments by Lemaire et al. [45] and Daley et al. [43], (b) comparison between the present reaction mechanism and the detailed mechanism by Silke et al. [5] for three equivalence ratios (0.5, 1.0, and 2.0).

and predictions using detailed mechanisms. Shock tube tests and engine experimental data available in the literature were employed in the validation, as described above. For comparison with shock tube ignition delay data, the calculations were performed with the SENKIN code [34] under constant volume conditions. Also, the predicted ignition delay times were compared with those obtained using other mechanisms available in the literature. The detailed mechanisms for tetradecane oxidation of Westbrook et al. [6], toluene oxidation of Bounaceur et al. [4] and Andrae et al. [42], cyclohexane oxidation of Silke et al. [5], ethanol oxidation of Marinov [55], DME oxidation of Fischer et al. [59] and Curran et al. [58], and MB oxidation of Fisher et al. [3] were chosen for the comparisons.

In order to confirm the repeatability of predictions for PRF oxidation, a comparison of ignition delay prediction between the MultiChem mechanism and the previous reduced PRF mechanism was also performed. Simulations of engine combustion were performed using the multi-dimensional KIVA-3 V code [73] coupled with the CHEMKIN library [74] and with physical sub-models developed at the Engine Research Center of the University of Wisconsin.

5.1. Validation of the reduced mechanism

Since the major interest of the present study was to develop a reduced multi-component chemistry mechanism to be used for auto-ignition processes of multi-component fuels, the mechanism validity was gauged by the ability to model auto-ignition of individual fuel components and multi-component sprays.

When no experimental data to compare and validate the reduced mechanism was available, the reduced mechanism was validated with the parent detailed mechanism.

5.1.1. PRF auto-ignition

Ignition delay predictions using the present MultiChem mechanism were validated with those obtained by the reduced PRF mechanism [11] for stoichiometric mixtures of *n*-heptane and iso-octane under various initial temperatures, as shown in Fig. 7. The simulations were performed at a pressure of 40 bar. For comparison, shock tube experimental data of Fieweger et al. [75] is included. As can be seen, the predictions by the present MultiChem mechanism are in excellent agreement with those by the reduced PRF mechanism, which confirms that the PRF oxidation branches are well represented in the new reduced mechanism.

Further improvement was made to the performance of heat release and species predictions by including additional reactions and by optimizing reaction rate constants of selected reactions. Heat release rate predictions of HCCI combustion of gas mixtures highly diluted with exhaust gas recirculation (O_2 = 8.58% at intake valve closure, $\phi_{overall} \sim 0.68$) were significantly improved, as shown in Fig. 8a. The PRF mechanism of Ra and Reitz [11] tends to show double-humps in heat release rate profiles due to excessive termination of active radicals before radical branching reactions (e.g., $H_2O_2(+m) = OH + OH(+m)$) take place. It is clearly seen in the figure that the double-hump behavior was eliminated by the present mechanism and the pressure profile becomes smoother during the main ignition period.

In addition, the UHC and CO emissions predictions were improved in the present mechanism. In Fig. 8b, emissions and gas temperature predictions are compared among the LLNL detailed mechanism, the PRF mechanism by Ra and Reitz [11], and the PRF mechanism in the present study for HCCI engine operation at various mixture equivalence ratios. Contours of crank angle at which, for each equivalence ratio, gas temperatures become 1200 and 1500 K, and UHC and CO emissions become 20 and 88 g/kg f, respectively, are plotted. The contours predicted by the present PRF mechanism, especially the UHC contour for rich mixtures, are in much better agreement with those by the detailed mechanism [38] than the previous mechanism [11].

5.1.2. n-Tetradecane auto-ignition

Ignition delay times of *n*-tetradecane/air mixtures at constant volume were simulated with the present MultiChem mechanism for two different equivalence ratios (ϕ = 1.0 and 0.5) at an initial pressure of 40 bar. The experimental measurements by Shen et al. [66] were used for comparison. Figure 9a shows comparison of predicted ignition delays using the present mechanism with the shock tube test data and predictions obtained using the detailed mechanisms of Westbrook et al. [6]. The present predicted ignition delays are in good agreement with experimental data for both equivalence ratios except for one stoichiometric mixture data point at low temperature (~870 K). However, for this condition, which falls in the NTC regime for other *n*-alkane fuels, the measured ignition delay time is much longer than corresponding values for other *n*-alkanes, especially *n*-heptane (see Fig. 9a, refer to [11]). Moreover, the ignition delays of *n*-tetradecane are reasonably expected to be faster than those of *n*-heptane, based on the reported CN numbers of the two fuels (CN_{nC7H16} = 52 vs. $CN_{nC14H30}$ = 93, [76]). More experimental data of *n*-tetradecane ignition delay at low temperatures would be desirable for better validation of reaction mechanisms. It is seen from the figure that the detailed mechanism tends to overpredict the measured ignition delay over the entire temperature range considered for both equivalence ratios. The ignition delay times of stoichiometric *n*-tetradecane/air mixtures are compared in Fig. 9b with those of stoichiometric *n*-heptane/air mixtures using the present reaction mechanism. The *n*-tetradecane ignition delays are predicted to be slightly faster than those of *n*-heptane, which is consistent with the results reported in Westbrook et al. [6] and the CN expectation.

5.1.3. Toluene auto-ignition

The toluene oxidation branch of the present reaction mechanism was validated with various experiments and predictions by detailed mechanisms. The shock tube experimental data by Bounaceur et al. [4] and Davidson et al. [67] were compared with predictions for toluene/O_2/Ar mixtures at high temperatures and toluene/air mixture at intermediate-to-high temperatures, respectively. In order to check the prediction performance for *n*-heptane/toluene/air mixtures at low-to-intermediate temperatures, the experiments by Herzler et al. [68] were used. In addition, the predictions obtained using detailed mechanisms available in the literature were compared with those by the present reaction mechanism.

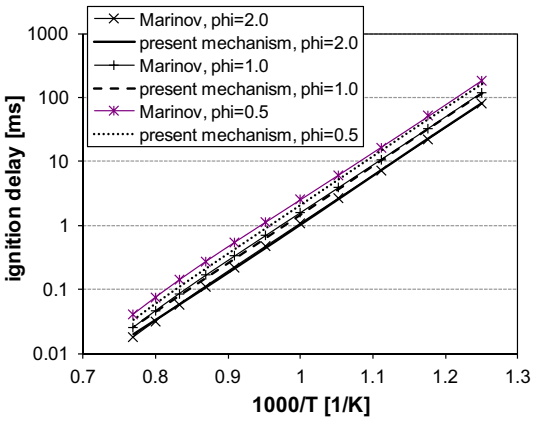

Fig. 13. Comparison of prediction of ignition delay times of ethanol oxidation with air at constant volume between the present reaction mechanism and a comprehensive mechanism [55]. Initial pressure is 40 bar.

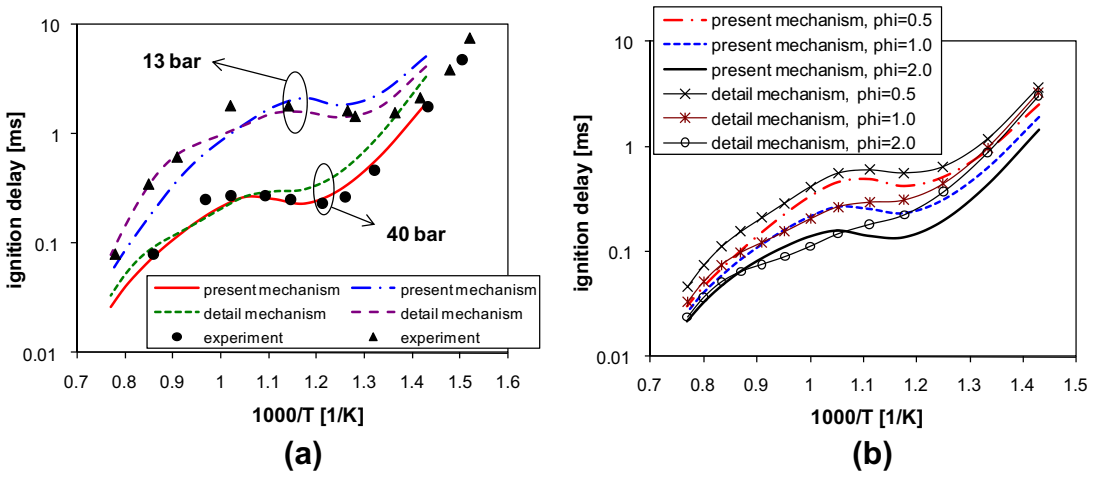

Fig. 14. Comparison of prediction of ignition delay times of DME oxidation with air at constant volume between the present reaction mechanism and a comprehensive mechanism [58,59]. Initial pressure is 40 bar.

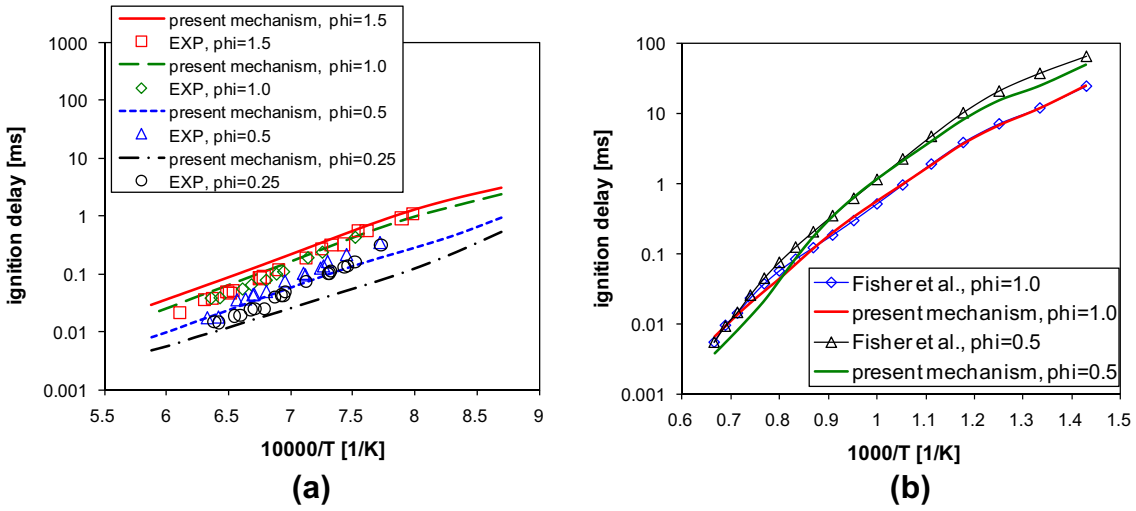

Fig. 15. Comparison of ignition delay time predictions between the present reaction mechanism and shock tube experiments by Dooley et al. [61] and predictions with a detailed mechanism by Fisher et al. [3]. (a) Comparison with shock tube data was for MB/O_2/Ar mixtures at an initial pressure of 4 atm, (b) comparison with detailed mechanism for MB/air mixtures at an initial pressure of 40 bar.

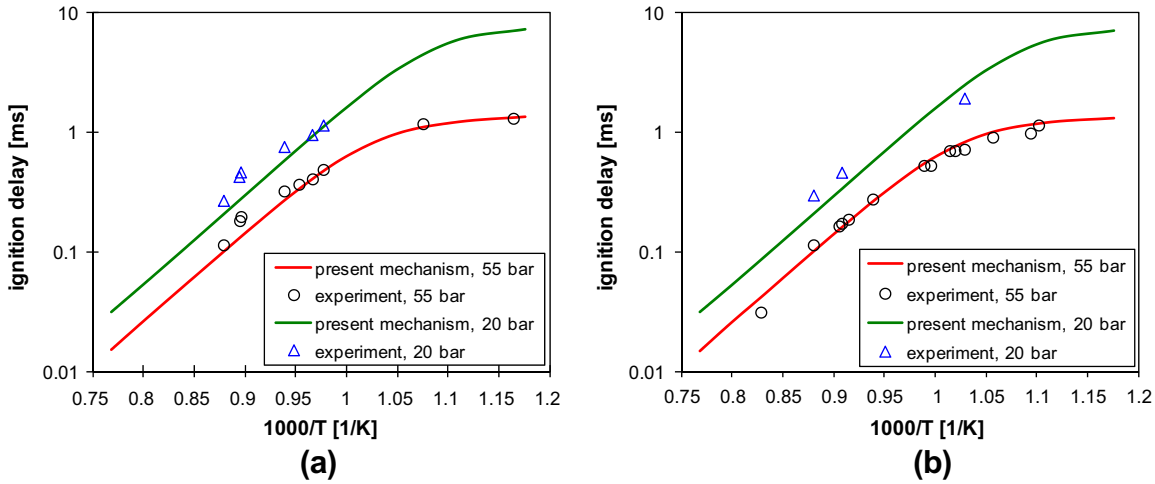

Fig. 16. Comparison of predicted ignition delay times with shock tube test data for gasoline surrogate compositions of Gauthier et al. [70]. Stoichiometric mixtures of the fuel in air were considered. (a) Surrogate-A: 63% iso-octane + 20% toluene + 17% *n*-heptane, (b) Surrogate-B: 69% iso-octane + 14% toluene + 17% *n*-heptane.

Ignition delay times of toluene/O_2/Ar mixtures were calculated at an initial pressure of 50 bar for two different equivalence ratios (0.5 and 1.0). In both cases, the toluene mole fraction was fixed at 1.25%. In Fig. 10a and b, predicted ignition delays under high initial temperature conditions are compared with experimental data and predictions by detailed mechanisms of Bounaceur et al. [4] and Andrae et al. [42]. The present reaction mechanism slightly overpredicts the ignition delay times compared to the experimental data. However, it is seen that the predicted ignition delays by the present reaction mechanism are in best agreement with the measured data and capture the trend of ignition delays excellently compared to the two detailed mechanisms.

Ignition delay times of toluene/air mixtures predicted by the present mechanism were also compared with experimental data for stoichiometric mixtures at 50 bar initial pressure and intermediate temperatures, as shown in Fig. 10c. Overall, the present reaction mechanism predicts ignition delay times and their trends with respect to initial temperature variation reasonably well, although it tends to overpredict ignition delays as the initial mixture temperature is decreased. The detailed mechanism by Andrae et al. [42] captures the ignition delay times quite well, while the mechanism by Bounaceur et al. tends to significantly overpredict.

In Fig. 10d, the performance of the three mechanisms are compared for stoichiometric toluene/air mixtures at an initial pressure of 40 bar over low-to-high temperature ranges. Compared to the ignition delay times of *n*-alkanes under similar conditions, toluene ignition delay times are predicted to be much longer. It is notable that no NTC behavior is seen in toluene oxidation over the entire temperature range considered. The predictions by the present reaction mechanism are in good agreement with those by Andrae et al. [42].

In order to validate the performance of the present reaction mechanism in predicting ignition delay times of *n*-heptane/toluene blended mixtures, auto-ignition of a mixture of 35% *n*-heptane and 65% toluene in air was simulated. In Fig. 11a stoichiometric ignition delay times are compared with shock tube experimental data for various initial pressures. Ignition delay times at 10 and 30 bar are reasonably well predicted by the present reaction mechanism, but the 50 bar case tends to be underpredicted. Due to the effects of the *n*-heptane oxidation pathways, a clear NTC behavior is seen in all three pressure cases. The present reaction mechanism also performs well for mixtures with equivalence ratio of 0.3, as shown in Fig. 11b. Overall, the experimental ignition delay times are well captured by the present reaction mechanism, although the ignition delay times in the lowest initial pressure case tend to be underpredicted at high temperatures.

5.1.4. Cyclohexane auto-ignition

The performance of the present reaction mechanism was validated with ignition delay measurements in a rapid compression machine by Lemaire et al. [45] and in shock tube tests by Daley et al. [43]. Ignition delay times of cyclohexane/air mixtures were

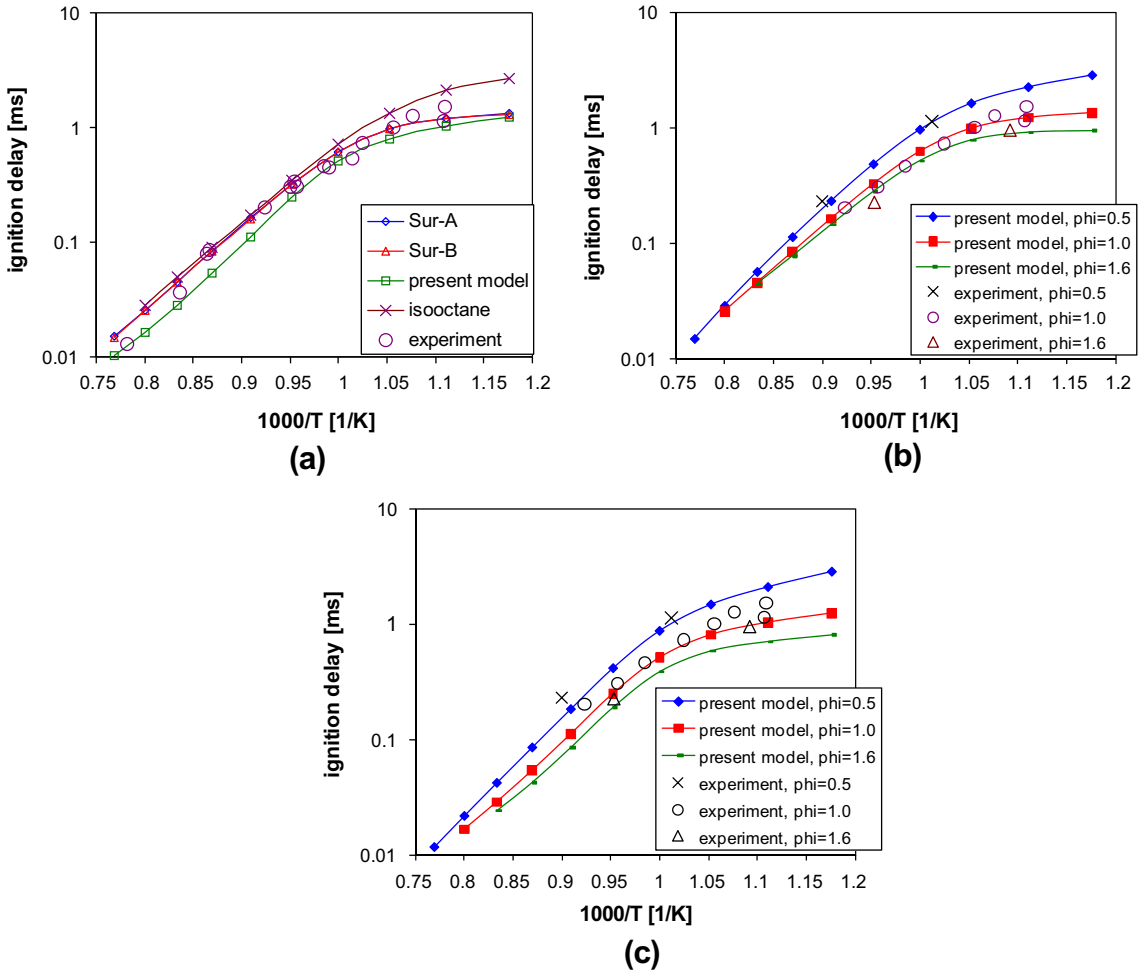

Fig. 17. Comparison of predicted ignition delay times with the shock tube test data for gasoline by Gauthier et al. [70]. Initial pressure 55 bar. (a) Ignition delay times of stoichiometric gasoline/air mixtures, (b) effect of equivalence ratio variation predicted using Surrogate-A composition, (c) effect of equivalence ratio variation predicted using the present 4-component model.

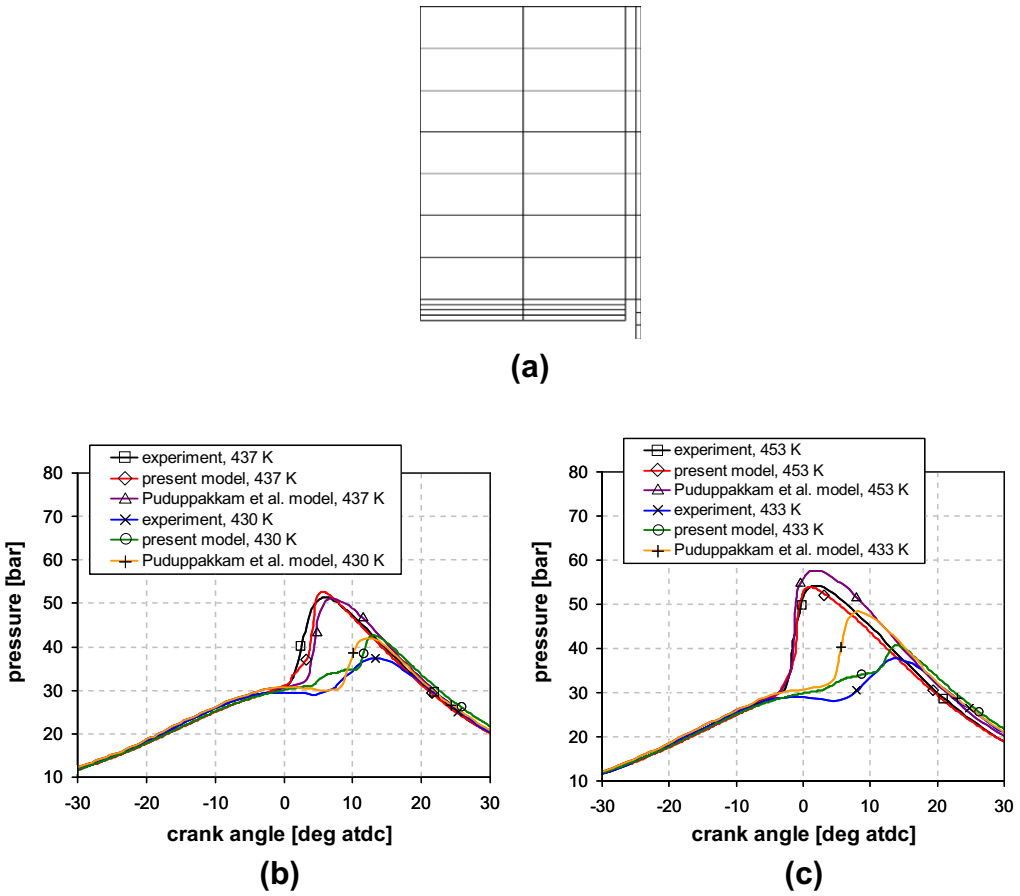

Fig. 18. Comparison of predicted pressure profiles in a gasoline HCCI engine with experiments and predictions by Puduppakkam et al. [17]. (a) 2-D computational grid used in the predictions using the present model, (b) Blend-1 for initial intake temperatures of 437 and 430 K, (c) Blend-2 for intake temperatures of 453 and 433 K.

calculated at an initial pressure of 12.5 bar. For comparison, ignition delay calculations using the detailed mechanism by Silke et al. [5] were performed for the same conditions. In Fig. 12a, predictions and measured data are compared for stoichiometric cyclohexane/air mixtures. Note that the RCM data, which was originally obtained in the pressure range of 11–14 atm, was scaled to 12.5 bar to be combined with the shock tube data. The ignition delays by the present reaction mechanism are in good agreement with the measurements except that it tends to underpredict the delays for very low temperatures, while the detailed mechanism overpredicts ignition delays over the low-to-intermediate temperature range. The NTC regime temperatures of cyclohexane oxidation at initial pressure of 12.5 bar are much lower than those of *n*-heptane and *n*-tetradecane at 40 bar (compare Fig. 9). It was found that the range of temperature corresponding to the NTC behavior in cyclohexane oxidation moves to higher temperatures as the initial pressure increases (not shown).

The effect of equivalence ratio variation was tested for the same initial pressure. In Fig. 12b, the predicted ignition delay times at three equivalence ratios (0.5, 1.0 and 2.0) are compared with those by the detailed mechanism. For all three equivalence ratio cases, the detailed mechanism tends to predict longer ignition delays, except for temperatures higher than around 1100 K. Overall, the effect of the equivalence ratio variation is seen to be similar in both mechanisms.

5.1.5. Ethanol auto-ignition

The performance of the present MultiChem mechanism for the auto-ignition of ethanol was validated by comparing the ignition delay times at constant volume for various initial temperature and equivalence ratios with those obtained using a comprehensive mechanism [55], as shown in Fig. 13. The ignition delay times of ethanol at relatively low temperatures are substantially longer that those of typical aliphatic components in gasoline and diesel fuels, as can be expected from its typical CN number (~10).

Over the entire temperature range considered, it is seen that the predictions by the present reaction mechanism are in good agree-

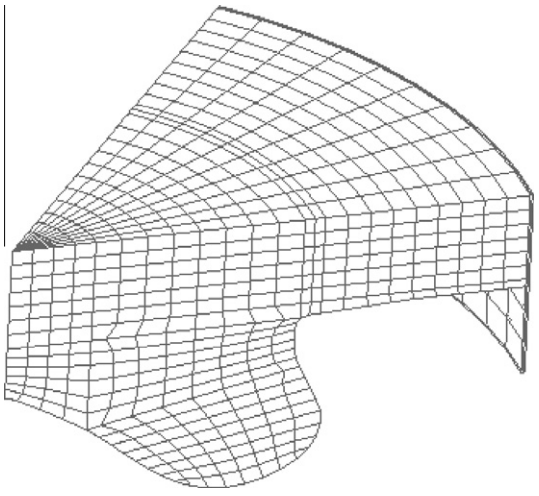

Fig. 19. Computational grid used in the engine simulations. 1/7th sector grid with 10,470 cells for DI diesel combustion simulation.

ment with those by the comprehensive mechanism, although there is slight discrepancy for lean mixtures at high initial temperatures.

5.1.6. DME auto-ignition

The performance of the MultiChem mechanism for the auto-ignition of DME was validated with the shock tube tests of Pfahl et al. [69]. In the experiments, ignition delay times of stoichiometric DME/air mixtures were measured at two different initial pressures (13 and 40 bar). Simulations of the ignition process at constant volume were performed for the two initial pressure conditions with the present reaction mechanism. For the comparison between the reduced and the detailed mechanism [58,59], ignition delay times at 40 bar initial pressure were calculated for various equivalence ratios.

Figure 14a shows comparisons of ignition delay with respect to initial temperature between measurements and predictions. For 40 bar initial pressure, ignition delay times predicted by the present reaction mechanism are in good agreement with the experimental data, while the detailed mechanism slightly overpredicts ignition delays in the low temperature range. On the contrary, the present reaction mechanism tends to overpredict ignition delay times at low temperatures, while it tends to underpredict at intermediate-to-high temperatures. It would be necessary to further optimize the pressure dependency of the reduced mechanism to improve the performance of the reduced mechanism.

The performance of the reduced mechanism in terms of equivalence ratio variation is compared with that of the detailed mechanism in Fig. 14b. Three equivalence ratios were considered. As the equivalence ratio increases, the ignition delay times shorten in both mechanisms. However, the variation of ignition delay times with equivalence ratio in the detailed mechanism case is smaller than that of the present reaction mechanism at low temperatures up to 850 K, while it becomes greater for temperatures higher than 900 K. It is interesting that the ignition delay behavior predicted by the reduced mechanism for equivalence ratio 2.0 mixtures shows the NTC behavior clearly, while the detailed mechanism shows only a gradual decrease of ignition delay times with increasing initial mixture temperature.

5.1.7. MB auto-ignition

The performance of the present reaction mechanism in ignition delay predictions of MB was validated with shock tube experimental data by Dooley et al. [61] and ignition delay times calculated using the detailed mechanism by Fisher et al. [3], which was the base mechanism for the MB oxidation branch in the present reaction mechanism. For detailed composition information of the mixtures, see Ref. [61].

In Fig. 15, ignition delay times of $MB/O_2/Ar$ mixtures at an initial pressure of 4 atm are compared for various equivalence ratios between predictions by the present mechanism and experimental data. For stoichiometric and rich mixtures, the present mechanism predicts the experimental ignition delay times reasonably well, while it tends to underpredict as the mixtures become leaner, especially at lower temperatures. However, when the performance of the present mechanism is compared with that of the comprehensive mechanism, the predictions by both mechanisms are in good agreement over the entire temperature range considered, as shown in Fig. 15b. Note that the MB oxidation mechanism was optimized to match the predictions by the comprehensive mechanism when it first was developed by Brakora et al. [10]. Therefore, further improvement of MB mechanism to match the experimental measurements would be desirable.

5.1.8. Gasoline auto-ignition

With the individual surrogate component mechanisms having been validated against ignition delay measurements and predictions of detailed mechanisms, the present reaction mechanism was further validated with experimental ignition delay measurements with known compositions of multi-component fuels. Ignition delay times at constant volume condition were calculated for the two iso-octane/toluene/*n*-heptane compositions proposed by Gauthier et al. [70] as a gasoline surrogate. In Fig. 16 the predicted ignition delay times at two different initial pressures are compared with the experimental data of Gauthier et al. The ignition delay times predicted by the present reaction mechanism are in excellent agreement with the measured values for both surrogate compositions.

In order to model the auto-ignition of multi-component gasoline, predictions by the present reaction mechanism were also performed using three other surrogate composition models. A new 4-component composition including cyclohexane to account for naphthenes on gasoline auto-ignition behavior was tested, along with the two surrogate compositions suggested by Gauthier et al. [70], as summarized in Table D1 [78].

The performance of the three composition models are compared with measured data in Fig. 17a. Ignition delay times of 100% iso-octane are plotted for comparison, as well. All calculations were done for stoichiometric mixtures at 55 bar initial pressure. Overall, Surrogate-A gives best agreement with measurements among the surrogate models. As was expected, 100% iso-octane showed the longest ignition delay times, especially at lower temperatures. The present 4-component model tends to slightly underpredict, which indicates that adjustment of the composition of the fuel mixture may be necessary for better agreement. However, the present 4-component

Table 4
Reaction rate constants of modified reactions for DI spray combustion simulations (both base and revised values are shown).

Reaction no.	Reaction		A	*n*	Ea (cal/mole)
14	$nC_7H_{16} + HO_2 = C_7H_{15} - 2 + H_2O_2$	Base	2.44E + 14	0.0	16950.0
		Revised	4.88E + 14	0.0	16950.0
17	$C_7H_{15}O_2 + O_2 = C_7KET12 + OH$	Base	1.54E + 14	0.0	18232.7
		Revised	2.30E + 14	0.0	18232.7
18	$C_7KET12 = C_5H_{11}CO + CH_2O + OH$	Base	9.01E + 14	0.0	41100.0
		Revised	1.80E + 15	0.0	41100.0
20	C_7H_{15}-2 = $C_2H_5 + C_2H_4 + C_3H_6$	Base	2.54E + 15	0.0	34600.0
		Revised	3.80E + 15	0.0	34600.0
23	$C_{14}H_{30} + HO_2 = C_{14}H_{29} + H_2O_2$	Base	1.01E + 14	0.0	17690.0
		Revised	1.51E + 14	0.0	17690.0
25	$C_{14}H_{29} + O_2 = C_{14}H_{29}O_2$	Base	3.77E + 12	0.0	0.0
		Revised	2.64E + 12	0.0	0.0
26	$C_{14}H_{29}O_2 + O_2 = C_{14}KET12 + OH$	Base	1.40E + 14	0.0	19232.7
		Revised	2.10E + 14	0.0	19232.7
27	$C_{14}KET12 = C_{12}H_{25}CO + CH_2O + OH$	Base	6.00E + 16	0.0	39000.0
		Revised	8.00E + 16	0.0	39000.0

model adequately captures the effects of equivalence ratio variation, as shown in Fig. 17c. While the present 4-component model still tends to slightly underpredict the ignition delay times compared to those of the Surrogate-A model (Fig. 17b), the trend of equivalence ratio variation is better captured by the present 4-component model, especially at higher temperatures. Therefore, the 4-component model can reasonably be expected to provide information about the effects of naphthenes on the auto-ignition of gasoline fuels better than the three-component Surrogate-A and -B models.

5.2. Validation of MultiChem mechanism with engine experiments

5.2.1. Gasoline HCCI combustion

The present reduced MultiChem mechanism was also tested against homogeneous charge compression ignition engine experiments by Puduppakkam et al. [17]. Two fuels, Blends 1 and 2 as listed in Table D2 [78] were considered with two different initial mixture temperatures for each fuel case. The operating conditions tested are listed in Table D3 [78]. To calculate the cylinder gas pressure as a function of crank angle, a coarse 2-dimensional CFD grid was employed, as shown in Fig. 18a. The simulations were performed using the KIVA code [73] coupled with the CHEMKIN library [74] for detailed chemistry calculation.

Figure 18 shows a comparison of the predicted pressure profiles with the experimental data and predictions obtained using a detailed mechanism including 1477 species and 6827 reactions by Puduppakkam et al. [17]. Overall, the ignition timings are reasonably well predicted by the present mechanism under both initial temperatures for both fuels. Predictions for higher intake temperatures were found to be in better agreement with the experiments and the predictions with the detailed mechanism in both fuel cases. The present reaction mechanism tends to show two distinct peaks in heat release rate during the main ignition period for the lower mixture temperature considered, as can be seen in the pressure profiles. Note that the temperature range of the gasoline surrogate shock tube tests for the validation of the present mechanism (see above) was higher than the gas temperatures found in the HCCI engine simulations. This indicates that further validation with shock tube tests at low-to-intermediate temperatures would be desirable for improving the performance of the present mechanism.

5.2.2. Validation of mechanism with DI diesel engine experiments

Finally, the present reduced MultiChem mechanism was applied to engine spray combustion simulations. Direct injection of sprays of model surrogate diesel fuel in a production engine [72] was simulated using a CFD computational grid with 10,470 cells in a 1/7th sector of the cylinder, as shown in Fig. 19. The engine was operated in the low temperature combustion regime with intake oxygen fraction of 9.5%. Table D4 [78] provides the details of the simulation conditions.

As pointed out by Ra and Reitz [11], in order to better simulate engine results the reaction branches of *n*-heptane and *n*-tetradecane in the present reaction mechanism were re-optimized for rich combustion conditions such that ignition delay predictions matched shock tube test data for mixtures at an equivalence ratio of 2.0. The necessary modification was made relatively simply using the information ignition delay curve sensitivity analysis (see Fig. 1). The standard and updated reaction rate constants are shown in Table 4. Although not shown, the predicted delay times of *n*-heptane/air at $\phi = 2.0$ using the re-optimized mechanism were also in good agreement with measured shock tube data. The *n*-tetradecane ignition delay times with $\phi = 2.0$ were slightly faster than those of *n*-heptane, as in the stoichiometric case.

An 8-component surrogate model was used to describe the physical properties of the sprays, as shown in Table 5. The composition was chosen to optimally match the distillation curves of the target fuel, as shown in Fig. 20a. Also, major physical properties (density, viscosity and heating value) were adjusted slightly to match measured values, using the methodology suggested by Ra et al. [77,79]. In order to calculate the chemistry of the multi-component fuel, the surrogate fuel components used for spray properties were grouped into chemistry-based surrogate components, as shown in Table 5. Cycloalkane, *n*-paraffin, and aromatic classes were considered and the cyclohexane, *n*-heptane, *n*-tetradecane, and toluene reactions of the present reaction mechanism were employed to model the combustion chemistry. Decalin oxidation was modeled with the cyclo-hexane mechanism. For the *n*-paraffins, components

Table 5
Model composition of surrogate diesel fuels for DI diesel engine tests.

8-Component spray model		Component in chemistry model
Component	Mass fraction (%)	
Cyclohexane	3.7	Cyclohexane
Decalin	6.4	
Toluene	5.0	Toluene
n-Decane	5.6	*n*-Heptane
n-Dodecane	20.9	
n-Tetradecane	25.9	*n*-Tetradecane
n-Hexadecane	16.6	
n-Octadecane	15.8	

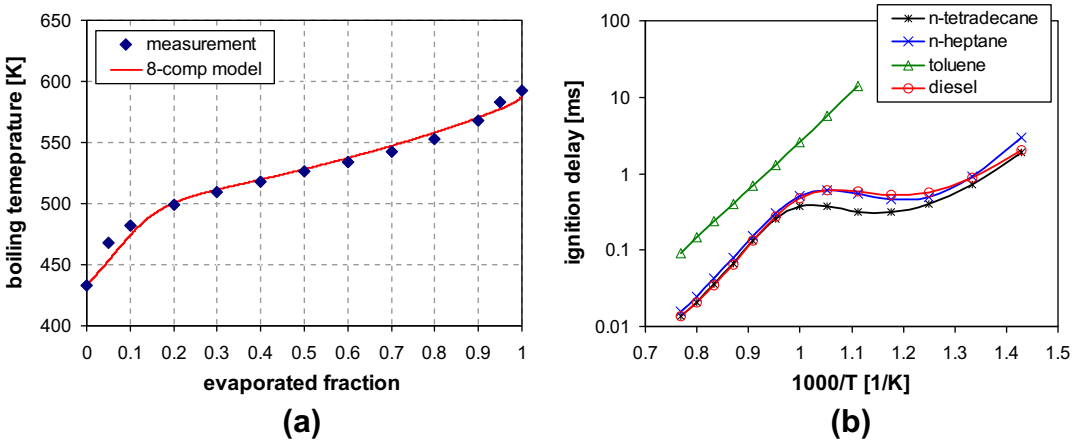

Fig. 20. Comparison of (a) measured and predicted distillation curves of a diesel fuel, (b) ignition delay times at constant volume, 40 bar initial pressure for stoichiometric mixtures of various fuels and air. Experimental distillation curves by Butts [72].

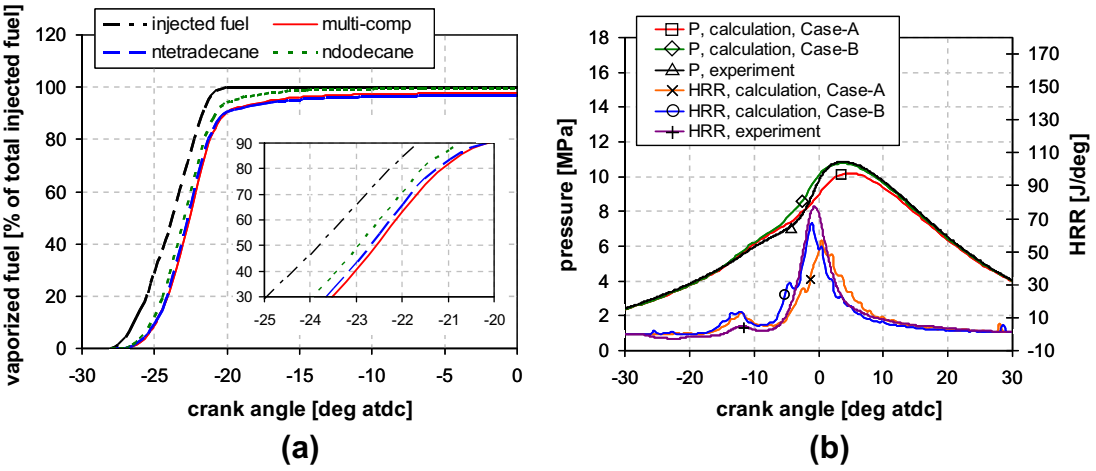

Fig. 21. Predictions of profiles of in-cylinder gas pressure, heat release rate and vaporized fuel. Pressures and heat release rates measured by Butts [72] are compared. (a) Comparison of profiles of total vaporized fuel for multi-component and two single component models, (b) pressure and heat release profiles.

lighter than *n*-tetradecane were described with *n*-heptane oxidation chemistry, while the components heavier than *n*-tetradecane are modeled with the *n*-tetradecane mechanism.

Redistribution of the grouped components was done after the chemistry calculation each time step based on the mass proportion of the components before the chemistry calculation, i.e., assuming that the reactivity of the components grouped into the same chemistry surrogate class was the same.

In Fig. 20b, the ignition delay times of stoichiometric diesel/air mixtures are compared with corresponding single component fuels. Using the present 4-component surrogate chemistry model, it is seen that the NTC behavior of the multi-component model fuel is well captured. It is interesting that, due to the interaction of oxidation reactions of the individual components, through both co-oxidation reactions and competition for common active radicals, the ignition delay times of the multi-component model fuel tend to follow those of *n*-tetradecane in the low and high temperature ranges, while they tend to be close to those of *n*-heptane in the NTC regime. Overall, the diesel ignition delay times predicted using the present 4-component surrogate model are very close to those of *n*-heptane.

Spray combustion of the multi-component diesel fuel was compared with single-component surrogate component (*n*-tetradecane and *n*-dodecane) cases. Figure 21a compares predicted profiles of vaporized fuel from non-reacting multi-component and single-component surrogate sprays. The vaporized fuel amounts were normalized with total injected fuel amount. *n*-Dodecane was chosen as a single component fuel since its molecular weight is close to the molecular weight of the present multi-component model fuel (170 g/mol) and *n*-tetradecane was chosen since it is widely used as a single-component surrogate for diesel fuels due to its close physical properties to diesel. Within the figure, the profiles are magnified for crank angles corresponding to 30–90% vaporized mass, as shown in the boxed figure.

It is seen that *n*-dodecane vaporizes faster than the other two fuels, which indicates that a single-component surrogate model may result in significantly different fuel vapor distributions than a multi-component fuel. The *n*-tetradecane model gives closer vaporization behavior to that of the multi-component model than the *n*-dodecane model. But the vaporized amounts are still slightly larger than those of the multi-component model. This is due to the fact that the multi-component fuel has a significant amount (32.4%) of components heavier than *n*-tetradecane, which have much lower vapor pressures and thus, vaporize much slower than *n*-tetradecane.

Profiles of pressure and heat release rate obtained using the re-optimized reduced mechanism are shown in Fig. 21b along with the experimental measurements. Two cases of chemistry surrogate component assignment were considered. In Case-A, the vapor fuel components were assigned to the chemistry surrogate components as listed in Table 5. In Case-B, decalin was allocated to *n*-heptane considering that the CN of decalin (~48) is much higher than that of cyclohexane (~13) [76] and is rather close to that of *n*-heptane (~52). The predicted timings of the cool flame and main ignition are good agreement with the measured data. The cool flame heat release tends to be overpredicted in both cases, which results in slightly faster pressure rise than the measurements during the main ignition period. In Case-A, the pressure rise rate during the main ignition is slower than Case-B and the peak cylinder pressure was significantly underpredicted. Modeling decalin oxidation with cyclo-hexane mechanism tends to give longer ignition delay times, especially at low-to-intermediate temperatures, thus could not capture the measured peak cylinder pressure timing. Note that, however, the predicted expansion pressures match well with the experimental data, which indicates that the fuels were eventually burned. On the contrary, Case-B captures the peak cylinder pressure and its timing well. This implies that the reactivity of the surrogate component for the naphthenes may need to be adjusted appropriately to better predict the ignition characteristics of the components included in the sprays.

6. Conclusions

A reduced chemical reaction mechanism for modeling the oxidation of multi-component fuels was developed using a combination of chemical lumping, graphical reaction flow analysis and elimination methods. Reduced oxidation mechanisms for *n*-tetradecane, toluene, cyclohexane, dimethyl ether, ethanol and methyl butanoate were combined with a reduced PRF oxidation mechanism to generate a multi-surrogate fuel chemical kinetic (MultiChem) mechanism that consists of 113 species and 487 reactions. The reactions involving low-C-number species and hydrogen oxidation were common in all the mechanisms. The mechanism reduction used available detailed mechanisms as the basis for the reduced chemistry and ignition delay curve sensitivity analysis was performed to identify important reaction steps and their effects on ignition. The reaction rate constants of reactions leading from each fuel component to common intermediate species were also optimized using the ignition delay curve sensitivity analysis.

The present MultiChem mechanism was validated with experimental measurements in shock tubes and available engine data. Also, the performance of the present mechanism was compared to that of other available mechanisms.

For each surrogate fuel mechanism, the predicted ignition delay times showed good agreement with experimental measurements under various temperatures, equivalence ratios and pressures. Also, ignition delay times of surrogate-blends were well predicted with the present reaction mechanisms. Simulations of gasoline HCCI combustion with a proposed surrogate composition successfully predicted ignition timings, cylinder gas pressures and heat release rates. Direct-injection diesel engine combustion simulations were performed to demonstrate the utility of the present MultiChem mechanism and to emphasize the importance of an accurate representation of the composition of a multi-component fuel for application to spray combustion.

Acknowledgment

This material is based on work supported by the Department of Energy Award DE-EE0000202.

Appendix A. Supplementary material

Supplementary data associated with this article can be found, in the online version, at doi:10.1016/j.combustflame.2010.07.019.

References

[1] H.J. Curran, P. Gauffuri, W.J. Pitz, C.K. Westbrook, Combust. Flame 114 (1998) 149–177.
[2] H.J. Curran, P. Gauffuri, W.J. Pitz, C.K. Westbrook, Combust. Flame 129 (2002) 253–280.
[3] E.M. Fisher, W.J. Pitz, H.J. Curran, C.K. Westbrook, Proc. Combust. Inst. 28 (2000) 1579–1586.
[4] R. Bounaceur, I. Da Costa, R. Fournet, F. Billaud, F. Battin-Leclerc, Experimental and modeling study of the oxidation of toluene, Int. J. Chem. Kinet. 37 (2005) 25–49.
[5] E.J. Silke, W.J. Pitz, C.K. Westbrook, M. Ribaucour, J. Phys. Chem. A 111 (2007) 3761–3775.
[6] C.K. Westbrook, W.J. Pitz, O. Herbineta, H.J. Curran, E.J. Silke, Combust. Flame 156 (2009) 181–199.
[7] K. Seshadri, M. Bollig, N. Peters, Combust. Flame 108 (1997) 518–536.
[8] N. Peters, G. Paczko, R. Seiser, K. Seshadri, Combust. Flame 128 (2002) 38–59.
[9] C. Hasse, M. Bollig, N. Peters, H.A. Dwyer, Combust. Flame 122 (2000) 117–129.
[10] J.L. Brakora, Y. Ra, R.D. Reitz, J. Mcfarlane, C.S. Daw, J. SAE Int. Fuels Lubr. 1 (2008) 675–702.
[11] Y. Ra, R.D. Reitz, Combust. Flame 155 (2008) 713–738.
[12] P. Dagaut, M. Cathonnet, Prog. Energy Combust. Sci. 32 (2006) 48–92.
[13] F. Buda, R. Bounaceur, V. Warth, P.A. Glaude, R. Fournet, F. Battin-Leclerc, Combust. Flame 142 (2005) 170–186.
[14] E. Ranzi, A. Frassoldati, S. Granata, T. Faravelli, Ind. Eng. Chem. Res. 44 (2005) 5170–5183.
[15] W.J. Pitz, N.P. Cernansky, F.L. Dryer, F.N. Egolfopoulos, J.T. Farrell, D.G. Friend, H. Pitsch, Development of an Experimental Database and Chemical Kinetic Models for Surrogate Gasoline Fuels, SAE Paper 2007-01-0175, 2007.
[16] J.T. Farrell, N.P. Cernansky, F.L. Dryer, D.G. Friend, C.A. Hergart, C.K. Law, R.M. McDavid, C.J. Mueller, A.K. Patel, H. Pitsch, Development of an Experimental Database and Kinetic Models for Surrogate Diesel Fuels, SAE Paper 2007-01-0201, 2007.
[17] K.V. Puduppakkam, L. Liang, C.V. Naik, E. Meeks, B.G. Bunting, Combustion and Emissions Modeling of a Gasoline HCCI Engine Using Model Fuels, SAE Paper 2009-01-0669, 2009.
[18] Y. Ra, R.D. Reitz, Int. J. Multiphase Flow 35 (2009) 101–117.
[19] Y. Ra, R.D. Reitz, Numerical study of multi-component spray combustion with a discrete multi-component fuel model, in: Proceedings of the 11th Triennial International Conference on Liquid Atomization and Spray Systems, July 2009.
[20] Y. Ra, R.D. Reitz, Numerical study of fuel composition effects on low temperature diesel combustion with a discrete multi-component vaporization model, in: Proceedings of the ASME Internal Combustion Engine Division 2009 Spring Technical Conference, ICES2009-76044, 2009.
[21] T.E. Daubert, R.P. Danner, Physical and Thermodynamic Properties of Pure Chemicals: Data Compilation, Hemisphere Pub. Corp, 1999.
[22] H. Rabitz, M. Kramer, D. Dacol, Annu. Rev. Phys. Chem. 34 (1983) 419–461.
[23] S. Vajda, P. Valko, T. Turanyi, Int. J. Chem. Kinet. 17 (1985) 55–81.
[24] T. Turanyi, J. Math. Chem. 5 (1990) 203–248.
[25] A.S. Tomlin, T. Turanyi, M.J. Pilling, Comprehensive Chemical Kinetics, Elsevier, 1997. p. 293.
[26] B. Bhattacharjee, D.A. Schwer, P.I. Barton, W.H. Green, Combust. Flame 135 (2003) 191–208.
[27] H. Wang, M. Frenklach, Combust. Flame 87 (1991) 365–370.
[28] S.S. Ahmed, F. Mauß, G. Moréac, T. Zeuch, Phys. Chem. Chem. Phys. 9 (2007) 1107–1126.
[29] H.S. Soyhan, T. LØvås, F. Mauss, A Stochastic Simulation of an HCCI Engine Using an Automatically Reduced Mechanism, ASME 2001-ICE-416, 2001.
[30] C.J. Montgomery, M.A. Cremer, J.Y. Chen, C.K. Westbrook, L.Q. Maurice, J. Propul. Power 18 (1) (2002) 192–198.
[31] T. Lu, C.K. Law, Combust. Flame 144 (2006) 24–36.
[32] A. Patel, S.C. Kong, R.D. Reitz, Development and Validation of a Reduced Reaction Mechanism for HCCI Engine Simulations, SAE Paper 2004-01-0558, 2004.
[33] XSENKPLOT: An Interactive Postprocessor for Numerical Simulations of Chemical Kinetics. <http://www.nist.gov/cstl/div836/xsenkplot>.
[34] A.E. Lutz, R.J. Kee, J.A. Miller, SENKIN: A FORTRAN Program for Predicting Homogeneous Gas Phase Chemical Kinetics with Sensitivity Analysis, Sandia Report SAND 87-8248, UC-4, 1988.
[35] C.K. Westbrook, Proc. Combust. Inst. 28 (2000) 1563–1577.
[36] S. Singh, S.C. Kong, R.D. Reitz, S.R. Krishnan, K. C. Midkiff, Modelling and Experiments of Dual-fuel Engine Combustion and Emissions, SAE Paper 2004-01-0092, 2004.
[37] R. Opat, Y. Ra, M.A. Gonzalez, R. Krieger, R.D. Reitz, D.E. Foster, R.P. Durrett, R.M. Siewert, Investigation of Mixing and Temperature Effects on HC/CO Emissions for Highly Dilute Low Temperature Combustion in a Light Duty Diesel Engine, SAE 2007-01-0193, 2007.
[38] https://www-pls.llnl.gov/?url=science_and_technology-chemistry-combustion-nc7h16.
[39] K. Owen, T. Coley, Automotive Fuels Reference Book, second ed., Society of Automotive Engineers, Inc., 1995.
[40] https://www-pls.llnl.gov/?url=science_and_technology-chemistry-combustion-c8c16_n_alkanes.
[41] A. Roubaud, R. Minetti, L.R. Sochet, Combust. Flame 121 (2000) 535–541.
[42] J.C.G. Andrae, P. Björnbom, R.F. Cracknell, G.T. Kalghatgi, Combust. Flame 149 (2007) 2–24.
[43] S.M. Daley, A.M. Berkowitz, M.A. Oehlschlaeger, Int. J. Chem. Kinet. 40 (10) (2008) 624–634.
[44] G. Dayma, P.A. Glaude, R. Fournet, F. Battin-Leclerc, Int. J. Chem. Kinet. 35 (2003) 273–285.
[45] O. Lemaire, M. Ribaucour, M. Carlier, R. Minetti, Combust. Flame 127 (2001) 1971–1980.
[46] A. El Bakali, M. Braun-Unkhoff, P. Dagaut, P. Frank, M. Cathonnet, Proc. Combust. Inst. 28 (2000) 1631–1638.
[47] M.E. Law, P.R. Westmoreland, T.A. Cool, J. Wang, N. Hansen, C.A. Taatjes, T. Kasper, Proc. Combust. Inst. 31 (2007) 565–573.
[48] S.G. Davis, C.K. Law, Combust. Sci. Technol. 140 (1998) 427–449.
[49] S.E. Klai, F. Baronnet, J. Chim. Phys. 90 (1993) 1951–1998.
[50] B. Sirjean, F. Buda, H. Hakka, P.A. Glaude, R. Fournet, V. Warth, F. Battin-Leclerc, M. Ruiz-Lopez, Proc. Combust. Inst. 31 (2007) 277–284.
[51] J.P. Orme, H.J. Curran, J.M. Simmie, J. Phys. Chem. A 110 (2006) 114–131.
[52] G. Vincent, P.M. Marquaire, O. Zahraa, J. Hazard. Mater. 161 (2009) 1173–1181.
[53] J. Peral, D.F. Ollis, J. Catal. 136 (1992) 554–565.
[54] M.R. Nimlos, E.J. Wolfrum, M.L. Brewer, J.A. Fennell, G. Bintner, Environ. Sci. Technol. 30 (1996) 3102–3110.
[55] N.M. Marinov, Chem. Kinet. 31 (1999) 183–220.
[56] A.M. El-Nahas, M.V. Navarro, J.M. Simmie, J.W. Bozzelli, H.J. Curran, S. Dooley, W. Metcalfe, J. Phys. Chem. A 111 (2007) 3727–3739.
[57] M.Y. Kim, S.H. Yoon, B.W. Ryu, C.S. Lee, Fuel 87 (2008) 2779–2786.
[58] H.J. Curran, S.L. Fisher, F.L. Dryer, Int. J. Chem. Kinet. 32 (2000) 741–759.
[59] S.L. Fischer, F.L. Dryer, H.J. Curran, Int. J. Chem. Kinet. 32 (2000) 713–740.
[60] W.K. Metcalfe, S. Dooley, H.J. Curran, J.M. Simmie, A.M. El-Nahas, M.V. Navarro, J. Phys. Chem. A 111 (2007) 4001–4014.
[61] S. Dooley, H.J. Curran, J.M. Simmie, Combust. Flame 153 (2008) 2–32.
[62] J. Andrae, D. Johansson, P. Björnbom, P. Risberg, G.T. Kalghatgi, Combust. Flame 140 (2005) 267–286.
[63] N.J. Kuprowicz, J.S. Erwin, S. Zabarnick, Fuel 83 (2004) 1795–1801.
[64] C.V. Naik, W.J. Pitz, C.K. Westbrook, M. Sjöberg, J.E. Dec, J. Orme, H.J. Curran, J.M. Simmie, Detailed Chemical Kinetic Modeling of Surrogate Fuels for Gasoline and Application to an HCCI Engine, SAE Paper 2005-01-3741, 2005.
[65] Y. Sakai, A. Miyoshi, M. Koshi, W.J. Pitz, Proc. Combust. Inst. 32 (2009) 411–418.
[66] H.-P.S. Shen, J. Steinberg, J. Vanderover, M.A. Oehlschlaeger, Energy Fuels 23 (2009) 2482–2489.
[67] D.F. Davidson, B.M. Gauthier, R.K. Hanson, Proc. Combust. Inst. 30 (2005) 1175–1182.
[68] J. Herzler, M. Fikri, K. Hitzbleck, R. Starkea, C. Schulza, P. Roth, G.T. Kalghatgi, Combust. Flame 149 (2007) 25–31.
[69] U. Pfahl, K. Fieweger, G. Adomeit, Proc. Combust. Inst. 26 (1996) 781–789.
[70] B.M. Gauthier, D.F. Davidson, R.K. Hanson, Combust. Flame 139 (2004) 300–311.
[71] G. Bikas, N. Peters, Combust. Flame 126 (2001) 1456–1475.
[72] R. Butts, MS Thesis, University of Wisconsin-Madison, 2008.
[73] A.A. Amsden, KIVA-3V, Release 2, Improvements to KIVA-3V, LA-UR-99-915, 1999.

[74] R.J. Kee, F.M. Rupley, J.A. Miller, CHEMKIN-II: A FORTRAN Chemical Kinetics Package for the Analysis of Gas Phase Chemical Kinetics, Sandia Report SAND 89-8009, 1989.
[75] K. Fieweger, R. Blumenthal, G. Adomeit, Combust. Flame 109 (1997) 599–619.
[76] M.J. Murphy, J.D. Taylor, R.L. McCormick, Compendium of Experimental Cetane Number Data, NREL Report: SR-540-36805, 2004.
[77] Y. Ra, R.D. Reitz, J. McFarlane, C.S. Daw, J. SAE Int. Fuels Lubr. 1 (2008) 703–718.
[78] Electronic Annex in the online version of this article.
[79] Y. Ra, R.D. Reitz, Numerical study of fuel composition effects on low temperature diesel combustion with a discrete multi-component vaporization model, in: Proceedings of the ASME Internal Combustion Engine Division 2009 Spring Technical Conference, ICES2009-76044, 2009.